Electromagnetic production of kaons from protons, and baryon electromagnetic form factors

Oren V. Maxwell

Department of Physics, Florida International University, University Park, Miami, Florida 33199, USA

The reactions $\gamma p \to K^+\Lambda$ and $ep \to e'K^+\Lambda$ have been investigated in a tree-level effective Lagrangian model that incorporates most of the well-established baryon resonances with spins up to $\frac{5}{2}$, four less well-established nucleon resonances with larger mass, and the $K^\star(892)$ and $K1(1270)$ resonances in the t channel. The off-shell structure of the electromagnetic vertices in electroproduction is incorporated by the addition of electromagnetic form factors. To achieve a good fit to the electroproduction data, it was found necessary to treat the ground-state hyperon form factors as adjustable parameters rather than simply equating them with the neutron form factors as was done in past studies. Photoproduction data consisting of unpolarized differential cross sections from the CLAS Collaboration, hyperon polarization asymmetries from CLAS, GRAAL, and SAPHIR, photon beam asymmetries from GRAAL and LEPS, and double polarization observables from CLAS were fit over the c.m. energy range from threshold up to 2.3 GeV. Electroproduction data for the virtual photoproduction structure functions σ_U, σ_T, σ_L, σ_{TT}, and σ_{LT} from the CLAS collaboration were fit over the ΣK c.m. energy range from threshold up to 2.3 Gev and for several values of q^2, the square of the virtual photon 4-momentum. For each intermediate resonance included, the fitted parameters in the photoproduction fit consist of the products of the coupling strengths at the electromagnetic and strong interaction vertices. In the electroproduction fit, there were, in addition, two form-factor parameters for each intermediate baryon in the s and u channels and one form factor parameter for each kaon resonance in the t channel. Results are presented for the fitted photoproduction and electroproduction observables and compared with the data for several sets of kinematical variables.

I. INTRODUCTION

The photoproduction of strangeness from the proton has been a subject of considerable interest since the mid 1980s. Much of the theoretical work, especially the earlier work, employed effective Lagrangian models [1–18], but several recent studies are based on coupled-channel approaches or chiral unitary frameworks [19–23]. There is currently a wealth of photoproduction data from several groups, including SAPHIR [24], LEPS [25], GRAAL [26,27], and CLAS [28–31]. Recently, a new photoproduction fit was published that incorporates much of this new data [32].

By contrast, the electroproduction of strangeness from the proton has received much less attention. Most of the recent data has been obtained at Jefferson Lab, either by the Hall C Collaboration [33] or by CLAS [34–36]. The earliest theoretical studies of electroproduction date from the mid 1970s, and were based on a simple Regge model [37]. More recent studies generally employ an effective Lagrangian model [2,4,7,9,10,14,38,39] and often treat both the electroproduction and photoproduction reactions together. There also exist updated Regge analyses of electroproduction [40] and studies based on chiral frameworks [23,41].

While electroproduction is more difficult to treat than photoproduction, both theoretically and experimentally, it involves virtual, rather than real, photons, and thus, has the potential to yield information not available from photoproduction. In particular, the reaction mechanism involves a longitudinal photon contribution and, within the context of effective Lagrangian models, is sensitive to the electromagnetic form factors of the intermediate hadronic resonances associated with the strangeness production reaction mechanism. In Ref. [32], it was suggested that these electromagnetic form factors could be studied within the framework of an effective Lagrangian

model using parameters fit to photoproduction data. The idea was that the photoproduction fit could be applied to electroproduction with just the addition of electromagnetic form factors at the virtual photon-hadronic vertices. The parameters associated with these form factors would then be fit to the electroproduction data. In other words, the basic reaction mechanism would be fixed by the photoproduction data; the electromagnetic form factors would be fixed by the electroproduction data.

That idea provided much of the motivation for the work reported here. We were also motivated by the desire to obtain a quantitative fit to recent electroproduction data comparable in quality with the fit of recent photoproduction data reported in Ref. [32]. Aside from the information they provide concerning the underlying interactions, such fits can be used to study strangeness-producing reactions involving more complex targets such as the deuteron and ^{3}He.

In practice, we found that the photoproduction data do not constrain the parameters of the photoproduction fit sufficiently to provide a good description of the longitudinal part of the electroproduction reaction. In principle, the Lorentz covariance of the reaction model determines the longiditudinal contributions to electroproduction once all the parameters of the model are fixed. Thus, if one were able to obtain a *unique* fit to the photoproduction data, one should be able to use that fit, with the addition of electromagnetic form factors, to describe the electroproduction reaction. The trouble is that the photoproduction fit reported in Ref. [32], while quantitative, is probably not unique. Different fits of comparable quality to the photoproduction data will generally yield quite different longitudinal contributions to electroproduction, since the photoproduction data only constrain the tranverse part of the reaction mechanism. We found that,

to obtain a good fit to the electroproduction data, it was necessary to adjust the parameters of the photoproduction fit by fitting the photoproduction data and the electroproduction data simultaneously. This was necessary even with electromagnetic form factors included in the electroproduction reaction model.

The remainder of this work is organized as follows: in the next section, we summarize the underlying reaction model used to describe both the photoproduction reaction, $\gamma p \rightarrow K^+ \Lambda$, and the electroproduction reaction, $ep \rightarrow e'K^+\Lambda$. For a more comprehensive discussion of this model, the reader should consult Ref. [32]. In Sec. III, the electroproduction reaction is discussed in more detail with detailed expressions given for the electroproduction structure functions.

The hadronic electromagnetic form factors are discussed in Sec. IV, both for the Born contributions in each reaction channel and for the contributions with intermediate hadronic resonances. In connection with these form factors, we note here that it has been a common practice in electroproduction studies to use the proton electromagnetic form factors in all s-channel contributions to the reaction and the neutron electromagnetic form factors in all the u-channel contributions. While this approximation has the virtue of simplicity, it is completely unjustified.

Section V presents details of the fitting procedure, including a summary of the data fit for both reactions and a list of the parameters to be fitted. Results for both the photoproduction reaction and the electroproduction reaction are presented in Sec. VI. Due to a sign error in the t-channel Born term, it was necessary to redo the photoproduction fit described in Ref. [32]. We then compare the photoproduction results obtained with two different fits: one obtained with the photoproduction data alone and the other with both photoproduction data and electroproduction data. Finally, electroproduction results obtained with the latter fit are compared with data from Ref. [35].

II. THE PHOTOPRODUCTION REACTION MODEL

The reaction model, consisting of s-channel, u-channel, and t-channel contributions, is depicted diagrammatically in Fig. 1. The s-channel contributions include the Born term with an intermediate proton and contributions in which an intermediate nucleon resonance is excited. The u-channel contributions include the Born term with an intermediate Λ and terms involving both the ground-state Σ baryon and intermediate hyperon resonances. Finally, in the t channel, the Born contribution is supplemented with contributions involving both $K^\star(892)$ and $K1(1270)$ exchange.

The general structure of the corresponding reaction amplitudes is given by the expressions

$$\hat{T}_s = \sum_{N^\star} \mathcal{V}_K^\dagger(p_K) D(p_s) \mathcal{V}_\gamma(p_\gamma), \tag{1}$$

$$\hat{T}_u = \sum_{Y^\star} \mathcal{V}_\gamma^\dagger(p_\gamma) D(p_u) \mathcal{V}_K(p_K), \tag{2}$$

and

$$\hat{T}_t = \sum_{K^\star} \mathcal{V}_{\gamma K}^\dagger(p_\gamma, p_t) D_t(p_t) \mathcal{V}_{p\Lambda}(p_t), \tag{3}$$
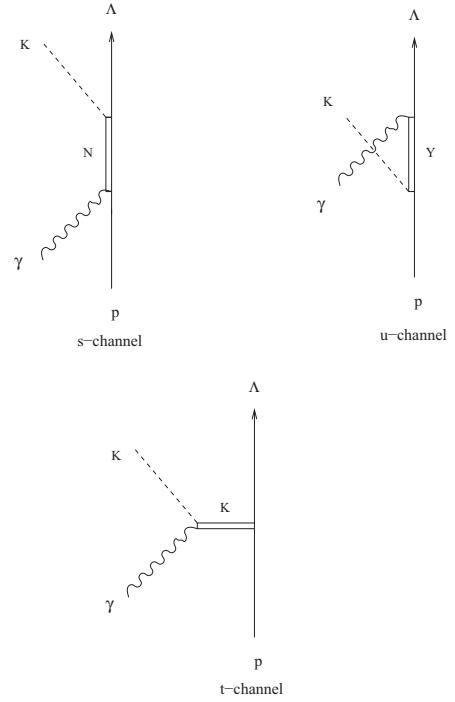

FIG. 1. Contributions to the amplitude for the reaction $\gamma p \rightarrow K^+\Lambda$.

where $p_s = p_\Lambda + p_K$, $p_u = p_\Lambda - p_\gamma$, and $p_t = p_\gamma - p_K$ are the intermediate 4-momenta in the s, u, and t channels, respectively, the $\mathcal{V}$'s designate the interaction vertices, and the D's the associated intermediate baryon and meson propagators. The particular forms of both the electromagnetic interaction vertices and the strong interaction vertices, as well as the propagators, depend explicitly on the spin and the parity of the intermediate hadron.

In the t channel, the interaction vertices are given by

$$\mathcal{V}_{\gamma K} = -e\epsilon \cdot (p_K - p_t) \tag{4}$$

and

$$\mathcal{V}_{p\Lambda} = g_{\Lambda K p} \gamma_5 \tag{5}$$

for an intermediate ground-state kaon (the t-channel Born term), by

$$\mathcal{V}_{\gamma K}^\mu = \frac{g_{\gamma K K^\star}}{m_{sc}} \epsilon^{\mu\nu\rho\lambda} \epsilon_\nu p_{\gamma\rho} p_{t\lambda} \tag{6}$$

and

$$\mathcal{V}_{p\Lambda}^\mu = \left(g_{\Lambda K^\star p}^V + \frac{g_{\Lambda K^\star p}^T}{m_p + m_\Lambda} \gamma \cdot p_t \right) \gamma^\mu \tag{7}$$

for an intermediate $K^\star(892)$ resonance and by

$$\mathcal{V}_{\gamma K}^\mu = \frac{g_{\gamma K K1}}{m_{sc}} \left(\epsilon \cdot p_t p_\gamma^\mu - p_\gamma \cdot p_t \epsilon^\mu \right) \tag{8}$$

and

$$\mathcal{V}_{p\Lambda}^\mu = \left(g_{\Lambda K1p}^V + \frac{g_{\Lambda K1p}^T}{m_p + m_\Lambda} \gamma \cdot p_t \right) \gamma^\mu \gamma_5 \tag{9}$$

for an intermediate $K1(1270)$ resonance. In these expressions ϵ denotes the photon polarization 4-vector and m_{sc} is a scaling mass, set equal to 1 GeV, introduced to make the electromagnetic coupling strengths dimensionless. For the t-channel resonance propagators we employ the expression

$$D_t = \frac{-g_{\mu\nu} + \frac{p_{t\mu}p_{t\nu}}{m_{K^\star}^2}}{p_t^2 - m_{K^\star}^2}, \tag{10}$$

where the label $K^\star$ now refers to either kaon resonance, and we note that no width is included since the intermediate energies in the t channel are always well below any possible decay thresholds.

In the s and u channels, we employ standard expressions for the interaction vertices that are associated with intermediate baryons of spin $\frac{1}{2}$. In particular, for positive-parity baryons, we use

$$\mathcal{V}_{K\frac{1}{2}^+}(p_K) = g\gamma_5 \tag{11}$$

and

$$\mathcal{V}_{\gamma\frac{1}{2}^+}(p_\gamma) = g_\gamma \epsilon_\mu i\sigma^{\mu\nu}(p_\gamma)_\nu \tag{12}$$

with

$$g_\gamma = \frac{e\kappa}{2m_B}, \tag{13}$$

where κ is defined by its relation to the transition magnetic moment,

$$\mu_T = \frac{e\kappa}{m_B + m_I}, \tag{14}$$

m_B is the mass of the incoming or outgoing baryon (m_p or m_Λ), and m_I is the mass of the intermediate baryon. The corresponding expressions for negative-parity intermediate baryons just have the γ_5 factor transposed from the strong interaction vertex to the electromagnetic vertex. For intermediate protons, there is an additional term,

$$\mathcal{V}_{\text{charge}}(p_\gamma) = e\gamma^\mu \epsilon_\mu, \tag{15}$$

arising from the proton's charge. For the spin-$\frac{1}{2}$ propagator, we employ, in agreement with other authors, a relativistic Breit-Wigner form,

$$D^{\frac{1}{2}}(p) = \frac{\gamma \cdot p + m_I}{p^2 - m_I^2 + im_I\Gamma_I}, \tag{16}$$

where the width Γ_I is nonzero only in the s channel.

For intermediate baryons of spin $\frac{3}{2}$, we employ the standard Rarita-Schwinger form for the spin-$\frac{3}{2}$ propagator and use forms for the corresponding vertices that are similar to those introduced in Ref. [10], but without off-shell terms. Other expressions have been employed for the spin-$\frac{3}{2}$ propagator [1], but these alternative expressions do not satisfy the differential equation that defines the propagator as a Green's function [42]. As for off-shell terms in the interaction vertices, the results of Ref. [10] suggest that these terms, as well as corresponding

terms in the propagator, have a relatively modest effect on calculated observables. For positive-parity spin-$\frac{3}{2}$ intermediate baryons, neglect of these terms yields the interaction vertices

$$\mathcal{V}_{K\frac{3}{2}^+}^\mu(p_K) = -\frac{g}{m_\pi}p_K^\mu, \tag{17}$$

and

$$\mathcal{V}_{\gamma\frac{3}{2}^+}^\mu(p_\gamma) = \left[\frac{g_1}{2m_B}\left(\epsilon^\mu \gamma \cdot p_\gamma - p_\gamma^\mu \gamma \cdot \epsilon\right) \right.$$
$$\left. + \frac{g_2}{4m_B^2}\left(\epsilon \cdot p_B p_\gamma^\mu - p_\gamma \cdot p_B \epsilon^\mu\right) \right]\gamma_5, \tag{18}$$

where p_B is the 4-momentum of the incoming or outgoing ground-state baryon. The corresponding negative-parity vertices just have the γ_5 factor transposed from one vertex to the other vertex. Note that we have employed the pion mass, rather than the kaon mass, to make the strong interaction coupling dimensionless.. The Rarita-Schwinger propagator is obtained by just multiplying the spin-$\frac{1}{2}$ propagator given by Eq. (16) on the right by the spin-$\frac{3}{2}$ projection operator

$$P_{\mu\nu}^{\frac{3}{2}} = g_{\mu\nu} - \frac{1}{3}\gamma_\mu\gamma_\nu + \frac{1}{3}\frac{p_\mu\gamma_\nu - p_\nu\gamma_\mu}{m_I} - \frac{2}{3}\frac{p_\mu p_\nu}{m_I^2}. \tag{19}$$

Our interaction model also includes intermediate baryons with spin $\frac{5}{2}$ in both the s and u channels. As reported in Ref. [32], this is necessary because there are several well-established resonances below 2 GeV that could have a significant impact on photoproduction observables within the kinematic range of the observations. For the spin-$\frac{5}{2}$ interaction vertices, we employ forms similar to those given in Ref. [9] but modified so as to be consistent with the forms adopted here for the spin-$\frac{3}{2}$ vertices. For the positive-parity intermediate resonances, the resulting expressions are

$$\mathcal{V}_{K\frac{5}{2}^+}^{\mu\nu}(p_K) = \frac{g}{m_\pi^2}p_K^\mu p_K^\nu \gamma_5 \tag{20}$$

and

$$\mathcal{V}_{\gamma\frac{5}{2}^+}^{\mu\nu}(p_\gamma) = \left[\frac{g_1}{2m_B}\left(\epsilon^\mu \gamma \cdot p_\gamma - p_\gamma^\mu \gamma \cdot \epsilon\right) \right.$$
$$\left. + \frac{g_2}{4m_B^2}\left(\epsilon \cdot p_B p_\gamma^\mu - p_\gamma \cdot p_B \epsilon^\mu\right) \right]\frac{p_\gamma^\nu}{m_\pi}. \tag{21}$$

As for the other s and u channel vertices, the corresponding negative-parity vertices just have the γ_5 factor transposed from one vertex to the other vertex. The corresponding propagator is constructed by multiplying the spin-$\frac{1}{2}$ propagator on the right by the spin-$\frac{5}{2}$ projector operator,

$$P_{\mu\nu,\mu'\nu'}^{\frac{5}{2}} = R_{\mu\nu,\mu'\nu'} - \frac{1}{5}P_{\mu\nu}P_{\mu'\nu'}$$
$$- \frac{1}{5}(P_{\mu\rho}\gamma^\rho\gamma^\sigma R_{\sigma\nu,\mu'\nu'} + P_{\nu\rho}\gamma^\rho\gamma^\sigma R_{\sigma\mu,\mu'\nu'}) \tag{22}$$

with

$$R_{\mu\nu,\mu'\nu'} = \frac{1}{2}(P_{\mu\mu'}P_{\nu\nu'} + P_{\mu\nu'}P_{\nu\mu'}), \tag{23}$$

where

$$P_{\mu\nu} = g_{\mu\nu} - p_\mu p_\nu/m_I^2. \tag{24}$$

As discussed in Ref. [32], the nucleon resonances excited in the s channel generally lie in kinematic regions where various decay channels are open. It is thus necessary to include widths in the s-channel resonance propagators, and these widths are usually required rather far off the resonance mass shell.

In Ref. [15] a model was proposed to dynamically generate widths off-shell by making use of the partial-width data summarized in the particle data tables [43]. The full width is first decomposed into a number of different decay channels. In each such channel, the off-shell energy and momentum dependence of the partial width is generated using an effective Lagrangian model with the required coupling strength adjusted to yield the empirical on-shell branching ratio for decay into that channel. The model treats two types of decays: two-body decays with stable decay products and decays in which one of the decay products is itself unstable. The latter decays are approximated as decays into either a ground-state baryon and a meson resonance or a ground-state meson and a baryon resonance. The corresponding widths are obtained by integrating the product of the relevant phase-space factor and a Breit-Wigner distribution function over the mass distribution of the unstable decay product. Reference [32] contains a detailed description of this model, including expressions for the phase-space factors and distribution function employed and values for all the required decay branching ratios.

In Ref. [32] the model was used to generate energy-dependent widths for all the three- and four-star nucleon resonances included in the fit. For these resonances the branching ratio data is generally good enough to obtain reasonably good estimates for the partial widths on the resonance mass shells. However, the model of Ref. [32] also included some larger-mass, less well-established nucleon resonances for which the partial-width data is limited. For these larger-mass resonances, the widths were simply treated as energy-independent parameters to be determined in the data fitting procedure. In the present work, we employ the same width prescription as used in Ref. [32]. In particular, we use the same on-shell branching ratios for the well-established nucleon resonances and the same energy-independent widths for the higher-energy nucleon resonances.

The matrix elements for the photoproduction reaction have the general structure

$$
\bar{u}_{M_\Lambda}(p_\Lambda)\hat{T}u_{M_p}(p_p) \\
= \bar{u}_{M_\Lambda}(p_\Lambda)[\hat{A} + \hat{B}\gamma_5 + \hat{C}\gamma^0 + \hat{D}\gamma^0\gamma_5]u_{M_p}(p_p), \quad (25)
$$

where p_p and M_p are the 4-momentum and spin projection of the proton, and p_Λ and M_Λ the 4-momentum and spin projection of the Λ. Detailed expressions for the operators $\hat{A}$, $\hat{B}$, $\hat{C}$, and $\hat{D}$ can be found in Ref. [32]. Equation (25) was evaluated by first converting it to the equivalent form involving Pauli spinors,

$$
\bar{u}_{M_\Lambda}(p_\Lambda)\hat{T}u_{M_p}(p_p) \\
= N_\Lambda N_p \chi_{M_\Lambda}^\dagger [(\hat{A}+\hat{C}) + (\hat{B} + \hat{D})\sigma \cdot \hat{p}_p + \sigma \cdot \hat{p}_\Lambda(\hat{D} - \hat{B}) \\
+ \sigma \cdot \hat{p}_\Lambda(\hat{C} - \hat{A})\sigma \cdot \hat{p}_p]\chi_{M_p}, \quad (26)
$$

TABLE I. Baryon resonances considered in the model

Resonance	I	J^P
$N(1440)$	$\frac{1}{2}$	$\frac{1}{2}^+$
$N(1520)$	$\frac{1}{2}$	$\frac{3}{2}^-$
$N(1535)$	$\frac{1}{2}$	$\frac{1}{2}^-$
$N(1650)$	$\frac{1}{2}$	$\frac{1}{2}^-$
$N(1675)$	$\frac{1}{2}$	$\frac{5}{2}^-$
$N(1680)$	$\frac{1}{2}$	$\frac{5}{2}^+$
$N(1700)$	$\frac{1}{2}$	$\frac{3}{2}^-$
$N(1710)$	$\frac{1}{2}$	$\frac{1}{2}^+$
$N(1720)$	$\frac{1}{2}$	$\frac{3}{2}^+$
$N(1900)$	$\frac{1}{2}$	$\frac{3}{2}^+$
$N(2000)$	$\frac{1}{2}$	$\frac{5}{2}^+$
$N(2080)$	$\frac{1}{2}$	$\frac{3}{2}^-$
$N(2200)$	$\frac{1}{2}$	$\frac{5}{2}^-$
$\Lambda(1405)$	0	$\frac{1}{2}^-$
$\Lambda(1670)$	0	$\frac{1}{2}^-$
$\Lambda(1820)$	0	$\frac{5}{2}^+$
$\Lambda(1830)$	0	$\frac{5}{2}^-$
$\Lambda(1890)$	0	$\frac{3}{2}^+$
$\Lambda(2110)$	0	$\frac{5}{2}^+$
$\Sigma(1385)$	1	$\frac{3}{2}^+$
$\Sigma(1775)$	1	$\frac{5}{2}^-$
$\Sigma(1915)$	1	$\frac{5}{2}^+$
$\Sigma(1940)$	1	$\frac{3}{2}^-$

where

$$
N = \sqrt{\frac{E+m}{2m}} \quad (27)
$$

and

$$
\hat{p} = \frac{\mathbf{p}}{E+m}, \quad (28)
$$

and then evaluating the Pauli matrix elements numerically.

Table I lists all the nucleon and hyperon resonances that were included in the fit of Ref. [32] and which have been included here. It should be noted that the analysis of Ref. [32] initially included a larger set of hyperon resonances, but that better results were achieved by reducing the number of resonances in the u channel (see Ref. [32] for details).

The set of parameters varied in the fit to the photoproduction observables consists of the products of coupling strengths at the two interaction vertices in each resonance contribution to the reaction amplitude. These products are defined by the relations

$$
F_{N^\star} = e\kappa_{pN^\star}g_{\Lambda KN^\star}, \quad F_{\Lambda^\star} = e\kappa_{\Lambda\Lambda^\star}g_{\Lambda^\star Kp}, \\
F_{\Sigma^\star} = e\kappa_{\Lambda\Sigma^\star}g_{\Sigma^\star Kp}, \quad (29)
$$

for the spin-$\frac{1}{2}$ baryons in the s and u channels, by

$$G^1_{N^\star} = g^{pN^\star}_1 g_{\Lambda K N^\star}, \quad G^2_{N^\star} = g^{pN^\star}_2 g_{\Lambda K N^\star},$$
$$G^1_{\Lambda^\star} = g^{\Lambda\Lambda^\star}_1 g_{\Lambda^\star K p}, \quad G^2_{\Lambda^\star} = g^{\Lambda\Lambda^\star}_2 g_{\Lambda^\star K p}, \qquad (30)$$
$$G^1_{\Sigma^\star} = g^{\Lambda\Sigma^\star}_1 g_{\Sigma^\star K p}, \quad G^2_{\Sigma^\star} = g^{\Lambda\Sigma^\star}_2 g_{\Sigma^\star K p}$$

for the spin-$\frac{3}{2}$ and spin-$\frac{5}{2}$ resonances in the s and u channels, by

$$F_K = e g_{\Lambda K p} \qquad (31)$$

for the ground state kaon in the t channel, and by

$$G^V_{K^\star} = g_{\gamma K K^\star} g^V_{\Lambda K^\star p}, \quad G^T_{K^\star} = g_{\gamma K K^\star} g^T_{\Lambda K^\star p} \qquad (32)$$

for the t-channel kaon resonances, where $e = 0.3029$ is the dimensionless electric charge. Note in Eqs. (29), that the $N^\star$, $\Lambda^\star$, and $\Sigma^\star$ subscripts refer to either the corresponding ground state baryon or a spin-$\frac{1}{2}$ resonance. Note also that in Eq. (31), we have corrected a sign error in Ref. [32]. For the proton, we also need the charge-coupling product. This is given by

$$F_{Cp} = e g_{\Lambda K p}. \qquad (33)$$

Values for the ground state coupling products can be obtained by combining SU(3) symmetry relations and SU(2) isospin coupling coefficients with data from the particle data tables. The symmetry relations yield the simple expressions

$$F_p = \kappa_p F_{Cp}, \quad F_\Lambda = \kappa_\Lambda F_{Cp}, \quad F_K = F_{Cp},$$
$$\frac{F_\Sigma}{F_\Lambda} = \frac{1}{\sqrt{3}} \frac{1 - 2\alpha}{1 - \frac{2}{3}\alpha} \frac{\kappa_\Lambda}{\kappa_{\Lambda\Sigma}}, \qquad (34)$$

where α is an SU(3) symmetry parameter that can be fixed using the empirical pion coupling strengths, and $\kappa_{\Lambda\Sigma}$ is the Λ-Σ transition magnetic-moment factor. For the various coupling factors appearing in these relations, we employ the same values as were used in Ref. [32]: $\kappa_p = -1.79$, $\kappa_\Lambda = -0.729$, $\kappa_{\Lambda\Sigma} = 1.91$, $\alpha = 0.625$, and $F_{Cp} = -1.98$, which yield the value $F_\Sigma = 0.934$. These values are consistent with a recent study based on a generalized Goldberger-Treiman relation used in conjunction with the Dashen-Weinstein sum rule [44]. For further discussion concerning the ground state couplings, the reader should consult Ref. [32]. Note that in the fits reported here, none of the ground-state couplings were varied.

III. ELECTROPRODUCTION

To describe the electroproduction reaction, we employ a formalism which is similar to that described in Ref. [39], but which differs from it in several respects. In particular, we include here baryon resonances with spins up to $\frac{5}{2}$, and we use a different method to evaluate the virtual photoproduction matrix elements. We have also incorporated a more sophisticated treatment of the baryon electromagnetic form factors.

The matrix element for the reaction $ep \rightarrow e'K^+\Lambda$ can be expressed, in the impulse approximation, as the product of a hadronic current and a leptonic current divided by q^2, the square of the 4-momentum of the exchanged virtual photon.

In particular,

$$\langle F|\hat{T}|I\rangle = \frac{l_\mu h^\mu}{q^2}. \qquad (35)$$

The lepton and hadronic currents are given by the relations

$$l_\mu = e \bar{u}_{M'}(p') \gamma_\mu u_M(p) \qquad (36)$$

and

$$h_\mu = e \bar{u}_{M_\Lambda}(p_\Lambda) \hat{t}_\mu u_{M_p}(p_p), \qquad (37)$$

where in the lepton current, p and p' are the incident and final electron 4-momenta and M and M' the corresponding electron spin projections.

After performing the electron spin projection sums, making use of the current conservation relation,

$$q_\mu h^\mu = 0, \qquad (38)$$

and imposing the extreme relativistic limit on the electron kinematics, the spin-summed square of the matrix element given by Eq. (35) can be expressed in terms of a summed matrix element for the virtual photoproduction of a Λ from a proton. In particular, one obtains

$$\frac{1}{4}\sum_{\text{spins}} |\langle F|\hat{T}|I\rangle|^2 = \frac{e^2}{2m_e^2 q^2} \frac{1}{\epsilon - 1} \sum_{M_\Lambda M_p} \frac{1}{2} |\langle f|\hat{t}_\gamma|i\rangle|^2, \qquad (39)$$

where $\langle f|\hat{t}_\gamma|i\rangle$ is the virtual photoproduction matrix element and

$$\epsilon = \left(1 - 2\frac{\mathbf{q}^2}{q^2} \tan^2\frac{\Psi}{2}\right)^{-1}, \qquad (40)$$

with Ψ denoting the electron scattering angle, is the transverse polarization of the virtual photon.

The differential cross section obtained from Eq. (39) is related to the corresponding virtual photoproduction cross section by the relation

$$\frac{d\sigma}{dE' d\Omega' d\Omega_K} = \frac{\alpha}{(2\pi)^4} \frac{p'}{(\epsilon - 1)q^2} \sqrt{\frac{(q_\mu p_p^\mu)^2 - q^2 m_p^2}{(p_\mu p_p^\mu)^2 - m_e^2 m_p^2}} \frac{d\sigma_\gamma}{d\Omega_K}, \qquad (41)$$

where α is the fine-structure constant, and the extreme relativistic limit has again been imposed on the electron kinematics. The virtual photoproduction cross section can be expressed most simply in the $K\Lambda$ c.m. system. In that frame,

$$\frac{d\sigma_\gamma}{d\Omega_K} = \frac{1}{(4\pi)^2} \frac{m_p m_\Lambda p_K}{|\mathbf{q}|s} \frac{1}{2} \sum_{\text{spins}} |\langle f|\hat{t}_\gamma|i\rangle|^2, \qquad (42)$$

where $\sqrt{s} = E_K + E_\Lambda$.

The simplest expression for the virtual photoproduction matrix element is obtained by choosing a coordinate system defined with respect to the lepton plane. If we choose the z axis in the direction of the virtual photon and the x axis so that the initial electron 3-momentum lies in the xz plane, then the spin-summed squared matrix element appearing in Eq. (42)

takes the form

$$
\frac{1}{2} \sum_{\text{spins}} |\langle f | \hat{t}_\gamma | i \rangle|^2
$$

$$
= \frac{1}{2} \sum_{M_\Lambda M_p} \left[\frac{1}{2}(\epsilon + 1)|h_x|^2 - \frac{1}{2}(\epsilon - 1)|h_y|^2 - \frac{q^2}{q_0^2}\epsilon|h_z|^2 \right.
$$

$$
\left. - \frac{1}{q_0}\sqrt{-\frac{q^2}{2}\epsilon(\epsilon + 1)}(h_x h_z^\star + h_x^\star h_z) \right], \quad (43)
$$

where q_0 denotes the fourth component of the virtual photon 4-momentum. Note in this expression that the squared 4-momentum, q^2, is negative.

While Eq. (43) involves components of the hadronic current defined with respect to the lepton plane, the hadronic current is more easily evaluated in a coordinate system defined with respect to the hadron plane. The two sets of components are related by a simple rotation. In particular, if we choose the x axis of the hadronic plane coordinate system so that the kaon 3-momentum lies in the xz plane, then we obtain

$$
h_x = \tilde{h}_x \cos\phi - \tilde{h}_y \sin\phi, \quad h_y = \tilde{h}_x \sin\phi + \tilde{h}_y \cos\phi,
$$

$$
h_z = \tilde{h}_z, \quad (44)
$$

where the $\tilde{h}$ are the hadron current components in the hadronic coordinate system, and ϕ is the angle between the hadron plane and the lepton plane.

The hadronic current matrix elements are defined by the expression

$$
\tilde{h} = \bar{u}_{M_\Lambda}(p_\Lambda)\hat{t}_{J^P}u_{M_p}(p_p), \quad (45)
$$

where J^P denotes the spin and parity of the intermediate hadron in a particular contribution to the matrix element. With the exception of the t-channel contribution involving an intermediate $K^\star(892)$ resonance, all of the matrix element operators have the general structure

$$
\hat{t}_{J^P} = \alpha_1 + \alpha_2\gamma_5 + \alpha_3\gamma^0 + \alpha_4\gamma^0\gamma_5
$$

$$
+ D_1\gamma + D_2\gamma\gamma_5 + D_3\gamma^0\gamma + D_4\gamma^0\gamma\gamma_5. \quad (46)
$$

The t-channel $K^\star(892)$ contribution has the form

$$
\hat{t}_{J^P} = \alpha_1 + \alpha_2\gamma_5 + \alpha_3\gamma^0 + \alpha_4\gamma^0\gamma_5
$$

$$
+ \beta_1 \times \gamma + \beta_2 \times \gamma\gamma_5 + \beta_3 \times \gamma^0\gamma + \beta_4 \times \gamma^0\gamma\gamma_5. \quad (47)
$$

The various α, β, and D quantities that appear in these relations are momentum-dependent operators that act within the 2×2 Pauli spinor space of the baryons. Detailed expressions for these operators with the electromagnetic form factors suppressed are given in the Appendix.

In Ref. [39], the hadronic matrix elements were evaluated by carrying out the Dirac algebra analytically and then evaluating the resulting Pauli matrix elements numerically. In the present work, where we include intermediate baryons with spin $\frac{5}{2}$ in the s and u channels, we have chosen to reduce the algebraic work required by directly evaluating the Dirac matrix elements numerically without first reducing them to Pauli form. We have checked that the two approaches agree numerically for the t-channel contributions to the matrix

elements and the s- and u-channel contributions with spin-$\frac{1}{2}$ and spin-$\frac{3}{2}$ intermediate baryons.

The virtual photoproduction cross section given by Eq. (42) can be conveniently decomposed into a number of structure functions according to the relation

$$
\frac{d\sigma_\gamma}{d\Omega_K} = \sigma_T + \epsilon\sigma_L + \epsilon\sigma_{TT}\cos 2\phi + \sqrt{\epsilon(\epsilon + 1)}\sigma_{LT}\cos\phi,
$$

$$
(48)
$$

where

$$
\sigma_T = \frac{1}{2}k \sum_{M_\Lambda M_p} \frac{1}{2}(|\tilde{h}_x|^2 + |\tilde{h}_y|^2),
$$

$$
\sigma_L = \frac{1}{2}k \sum_{M_\Lambda M_p} \frac{1}{2}\frac{-q^2}{q_0^2}|\tilde{h}_z|^2,
$$

$$
\sigma_{TT} = \frac{1}{2}k \sum_{M_\Lambda M_p} \frac{1}{2}(|\tilde{h}_x|^2 - |\tilde{h}_y|^2),
$$

$$
\sigma_{LT} = -k \sum_{M_\Lambda M_p} \frac{1}{q_0}\sqrt{\frac{-q^2}{2}}\Re(\tilde{h}_x\tilde{h}_z^\star), \quad (49)
$$

with

$$
k = \frac{m_p m_\Lambda p_K}{16\pi^2|\mathbf{q}|s}. \quad (50)
$$

It should be noted that this decomposition is consistent with that used in most experimental studies of the reaction $ep \rightarrow e'K^+\Lambda$, but differs slightly from that used in many theoretical studies, including that of Ref. [39].

In practice it has proved difficult experimentally to separate the transverse and longitudinal structure functions (σ_T and σ_L), with the result that, over most of the kinematic range considered, data exists only for the combined structure function,

$$
\sigma_U = \sigma_T + \epsilon\sigma_L. \quad (51)
$$

In contrast with σ_T and σ_L, which do not depend on the incident electron energy, σ_U does depend on the incident electron energy through its dependence on the polarization parameter ϵ.

IV. ELECTROMAGNETIC FORM FACTORS

Because of the off-shell nature of the exchanged photon, effective Lagrangian treatments of electroproduction require the use of electromagnetic form factors at the hadronic photon vertices. While the nucleon electromagnetic form factors have been studied extensively, there currently exists little information regarding the electromagnetic form factors of strange baryons or nucleon resonances.

The sensitivity of electroproduction observables to t-channel electromagnetic form factors has been examined in some detail [9,45], but very little attention has been paid to the form factors in the s and u channels. In fact, most previous studies of electroproduction have made use of an extremely crude model for the baryon electromagnetic form factors in which the proton form factor is employed for all

charged baryons and the neutron form factor for all neutral baryons. Such a prescription is completely unjustified for the baryon resonances, and, as pointed out in Ref. [38], the neutron magnetic form may not even provide a good representation of the Λ magnetic form factor, much less the form factors of the hyperon resonances. Indeed, in the present study, we were unable to find a quantitative fit to electroproduction data with the neutron form factor used to represent the Λ one.

In Ref. [39] a slightly more sophisticated model was introduced in which the baryon resonance form factors were supplemented by an adjustable multiplicative factor. The purpose of this model was not to obtain a quantitative fit to electroproduction data, but rather to study the sensitivity of calculated electroproduction observables to the baryon form factors. In fact, the results reported in that reference indicate that, depending on the kinematics, certain of the observables can be quite sensitive to the baryon electromagnetic form factors.

With the results of Ref. [39] in mind, we have adopted in the present work a model in which all of the hadronic electromagnetic form factors are varied except for those associated with an intermediate ground-state kaon or an intermediate proton. For the kaon form factor, we employ a parametrization based on a relativistic quark model [46], which was among those considered in Ref. [9]. It has the form

$$F_K(q^2) = \alpha_K \frac{\Lambda_1^2}{\Lambda_1^2 - q^2} + (1 - \alpha_K)\left(\frac{\Lambda_2^2}{\Lambda_2^2 - q^2}\right)^2 \quad (52)$$

with $\alpha_K = 0.398$, $\Lambda_1 = 0.642$ GeV, and $\Lambda_2 = 1.386$ GeV.

For the proton electromagnetic form factors, we conform with previous studies in adopting the proton form factors obtained by Gari and Krumpelmann using an extended vector meson dominance model [47]. Within that model, the charge and magnetic form factors are expressed as linear combinations of isoscalar and isovector contributions. The isoscalar contributions are attributed to ω-meson exchange modified by a perturbative QCD term, while the isovector contributions are attributed to ρ-meson exchange modifed by a perturbative QCD term. The parameters of the model, which include the ω- and ρ-meson coupling strengths and several form-factor mass parameters, were adjusted to fit nucleon electromagnetic data. Further details of the model, including parameter values, can be found in Ref. [39]. Here we employ the same parameter values as were used in that reference.

All of the remaining electromagnetic form factors contain parameters that are fit to electroproduction data. In the t channel, the kaon resonance form factors used here have the form

$$F_{K^\star}(q^2) = \frac{\Lambda_{K^\star}^2}{\Lambda_{K^\star}^2 - q^2}, \quad (53)$$

where the subscript $K^\star$ refers to either of the intermediate kaon resonances included in the t-channel contribution to the reaction amplitude.

For an intermediate Σ baryon in the u channel and for all the intermediate baryon resonances in the s and u channels,

we adopt the somewhat more versatile form

$$F(q^2) = \frac{1}{1 + \alpha} \frac{\Lambda^2}{\Lambda^2 - q^2}\left(1 + \alpha \frac{\Lambda^2}{\Lambda^2 - q^2}\right), \quad (54)$$

which contains two adjustable parameters, α and Λ, for each intermediate baryon. Note that for real photons with $q^2 = 0$, F is normalized to unity, so that the corresponding electromagnetic vertex has a strength equal to its value in the photoproduction reaction.

For the u-channel Born term, which involves an intermediate Λ baryon, there are both charge and magnetic contributions to the reaction amplitude. As for the other intermediate baryons, the Λ magnetic form factor is normalized to unity for $q^2 = 0$; however, the Λ charge form factor must reduce to zero for $q^2 = 0$ since the Λ has no charge. To satisfy this latter requirement, we define two form factors for the Λ, F_1 and F_2, each with the form given by Eq. (54). We then define the linear combinations

$$F_{\Lambda 1}(q^2) = \frac{1}{2}[F_1(q^2) - F_2(q^2)],$$
$$F_{\Lambda 2}(q^2) = \frac{\kappa_\Lambda}{2}[F_1(q^2) + F_2(q^2)], \quad (55)$$

where κ_Λ is the Λ magnetic moment parameter. In terms of these combinations, the charge and magnetic form factors of the Λ are given by

$$F_C(q^2) = F_{\Lambda 1}(q^2) - \tau_\Lambda F_{\Lambda 2}(q^2)],$$
$$F_M = \frac{1}{\kappa_\Lambda}[F_{\Lambda 1}(q^2) + F_{\Lambda 2}(q^2)], \quad (56)$$

with

$$\tau_\Lambda = \frac{q^2}{4m_\Lambda^2}. \quad (57)$$

Note that at $q^2 = 0$, $F_{\Lambda 1}$ and $F_{\Lambda 2}$ reduce to zero and κ_Λ, respectively, so that F_C and F_M reduce to zero and unity, respectively, as required.

An important issue regarding the electromagnetic form factors is the requirement that the hadronic current satisfy the current-conservation condition given by Eq. (38). Not only is current conservation necessary for gauge invariance, but since it has been used explicitly to fix the time component of the hadronic current, its violation will result in unphysical singularities in the reaction amplitude whenever the time component of the virtual photon 4-momentum vanishes. All of the contributions to the amplitude individually satisfy the current-conservation requirement with the exception of the Born charge contributions. Thus, except for the Born charge contributions, the addition of form factors at the electromagnetic vertices will not violate current conservation. For the charge contributions, in the absence of form factors, current conservation is satisfied by the sum of the t-channel Born term (kaon exchange) and the proton charge term (the u-channel charge term vanishes in the absence of form factors). This happens because the coupling products associated with these two terms are identical in the absence of form factors. Obviously, with the addition of form factors, the current-conservation condition will no longer be satisfied by these

terms, since there is no reason to expect the proton and kaon electromagnetic form factors to be the same.

One method to resolve this difficulty, as suggested in Ref. [48], is to introduce counter terms in the charge contributions to the amplitude. These are chosen so that, in the limit $q^2 \to 0$, one just recovers the usual charge contributions without form factors. In particular, we employ the expressions

$$\hat{t}^\mu_{ch} = e F_C(q^2)\gamma^\mu + [1 - F_C(q^2)]\frac{q^\mu}{q^2}\gamma \cdot q \quad (58)$$

for the proton charge vertex,

$$\hat{t}^\mu_{ch} = e F_C(q^2)\left[\gamma^\mu - \frac{q^\mu}{q^2}\gamma \cdot q\right] \quad (59)$$

for the Λ charge vertex, and

$$\hat{t}^\mu_K = e F_K(q^2)\left(2p^\mu_K - q^\mu\right)$$
$$+ [1 - F_K(q^2)]\left(\frac{2p_K \cdot q}{q^2} - 1\right)q^\mu \quad (60)$$

for the kaon electromagnetic vertex. Note here that, in the limit $q^2 \to 0$, the proton and kaon form factors both reduce to unity, and the Λ form factor reduces to zero.

V. FITTING PROCEDURE

As mentioned in the introduction, we were not able to achieve a quantitative fit to electroproduction data without adjusting the parameters obtained by fitting the photoproduction data alone. Thus, we refit the photoproduction parameters, consisting of all the resonance coupling products defined by Eqs. (29), (30), and (32), simultaneously to both photoproduction and electroproduction data. In addition to the photoproduction parameters, the set of form-factor coupling and mass parameters appearing in Eqs (53)–(55), was fit to the electroproduction data.

We employed the same set of photoproduction data in our fit as was used in Ref. [32]. This consists of the most recent CLAS data for the differential cross section [30], given by

$$\frac{d\sigma}{d\Omega} = \frac{1}{(2\pi)^2}\frac{m_p m_\Lambda p_F}{4E_\gamma s}\frac{1}{4}\sum_{\text{spins}}|\langle F|\hat{T}|I\rangle|^2 \quad (61)$$

in the center-of-momentum (c.m.) frame, where p_F is the outgoing 3-momentum in the c.m. and $s = W^2$ is the squared c.m. energy, plus CLAS [28], SAPHIR [24], and GRAAL [26] data for the hyperon polarization asymmetry P, GRAAL [26] and LEPS [25] data for the photon beam asymmetry Σ, and CLAS [31] data for the double polarization observables C_x and C_z. The hyperon and photon asymmetries are defined by the relations

$$P = \frac{d\sigma^+_\Lambda - d\sigma^-_\Lambda}{d\sigma^+_\Lambda + d\sigma^-_\Lambda}, \quad (62)$$

where the superscripts $^+$ and $^-$ refer to spin projections above and below the scattering plane, and

$$\Sigma = \frac{d\sigma^\perp_\Lambda - \sigma^\parallel_\Lambda}{d\sigma^\perp_\Lambda + \sigma^\parallel_\Lambda}, \quad (63)$$

TABLE II. Fit results for the coupling strength products. For each hadron, the first set of numbers is from the fit to both photoproduction and electroproduction data; the second set of numbers is from the fit to the photoproduction data only.

Spin-$\frac{1}{2}$ resonances			
$N(1440)$	$F_{N^\star}$	3.2545	2.7943
$N(1535)$	$F_{N^\star}$	0.4375	-0.0374
$N(1650)$	$F_{N^\star}$	-0.0484	0.0809
$N(1710)$	$F_{N^\star}$	0.0941	0.0445
$\Lambda(1405)$	$F_{\Lambda^\star}$	-3.2802	-7.9160
$\Lambda(1670)$	$F_{\Lambda^\star}$	4.4016	9.2854
Spin-$\frac{3}{2}$ resonances			
$N(1520)$	$G^1_{N^\star}$	-0.7442	-1.3233
	$G^2_{N^\star}$	-0.5355	-1.1888
$N(1700)$	$G^1_{N^\star}$	-0.0970	0.2417
	$G^2_{N^\star}$	-0.0675	0.0985
$N(1720)$	$G^1_{N^\star}$	-0.0020	-0.0643
	$G^2_{N^\star}$	-0.3068	-0.4057
$N(1900)$	$G^1_{N^\star}$	0.0210	-0.0077
	$G^2_{N^\star}$	-0.0146	-0.1070
$N(2080)$	$G^1_{N^\star}$	-0.0066	0.0030
	$G^2_{N^\star}$	0.0012	0.0071
$\Lambda(1890)$	$G^1_{\Lambda^\star}$	-1.6976	-5.5716
	$G^2_{\Lambda^\star}$	-7.9940	-7.2097
$\Sigma(1385)$	$G^1_{\Sigma^\star}$	0.1278	2.0140
	$G^2_{\Sigma^\star}$	5.3970	4.0580
$\Sigma(1940)$	$G^1_{\Sigma^\star}$	1.3050	-1.7048
	$G^2_{\Sigma^\star}$	0.2441	-3.5932
Spin-$\frac{5}{2}$ resonances			
$N(1675)$	$G^1_{N^\star}$	-0.0031	-0.0037
	$G^2_{N^\star}$	-0.0095	0.0076
$N(1680)$	$G^1_{N^\star}$	0.0251	0.0553
	$G^2_{N^\star}$	0.0012	0.0583
$N(2000)$	$G^1_{N^\star}$	-0.0172	-0.0318
	$G^2_{N^\star}$	-0.0110	-0.0340
$N(2200)$	$G^1_{N^\star}$	-0.0001	-0.0005
	$G^2_{N^\star}$	-0.0004	-0.0020
$\Lambda(1820)$	$G^1_{\Lambda^\star}$	-0.1643	0.3395
	$G^2_{\Lambda^\star}$	-1.8779	-4.5875
$\Lambda(1830)$	$G^1_{\Lambda^\star}$	-0.0875	-0.5155
	$G^2_{\Lambda^\star}$	-0.1653	-0.4905
$\Lambda(2110)$	$G^1_{\Lambda^\star}$	-0.1539	-0.1382
	$G^2_{\Lambda^\star}$	-1.5859	-3.5863
$\Sigma(1775)$	$G^1_{\Sigma^\star}$	0.0730	0.4655
	$G^2_{\Sigma^\star}$	0.1749	0.4809
$\Sigma(1915)$	$G^1_{\Sigma^\star}$	0.3204	-0.2569
	$G^2_{\Sigma^\star}$	3.4085	8.0386
t-channel resonances			
$K(892)$	$G^V_{K^\star}$	3.2840	3.2860
	$G^T_{K^\star}$	0.9215	-0.1044
$K(1270)$	$G^V_{K^\star}$	1.3698	2.2410
	$G^T_{K^\star}$	-3.4497	-1.7332

where $\perp$ and $\parallel$ refer to polarization vectors perpendicular and parallel to the scattering plane respectively. The double
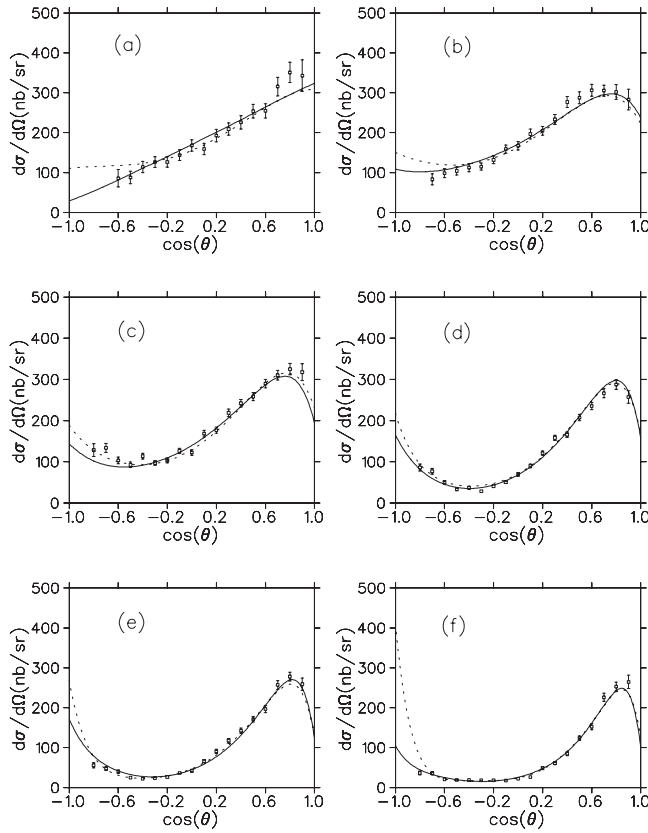
FIG. 2. Differential cross section vs. $\cos(\theta)$ for (a) $W = 1.727$ GeV, (b) $W = 1.832$ GeV, (c) $W = 1.920$ GeV, (d) $W = 2.028$ GeV, (e) $W = 2.120$ GeV, and (f) $W = 2.217$ GeV, where θ is the c.m. scattering angle and W is the c.m. energy. The solid curve was obtained by fitting both photoproduction and electroproduction data, the dashed curve by fitting just the photoproduction data. Data are from Ref. [30].

FIG. 3. Hyperon polarization asymmetry vs. $\cos(\theta)$ for (a) $W = 1.730$ GeV, (b) $W = 1.835$ GeV, (c) $W = 1.934$ GeV, (d) $W = 2.029$ GeV, (e) $W = 2.120$ GeV, and (f) $W = 2.228$ GeV, where θ is the c.m. scattering angle and W is the c.m. energy. The solid curve was obtained by fitting both photoproduction and electroproduction data, the dashed curve by fitting just the photoproduction data. Data are from Ref. [28].

polarization observables are given by

$$C_{i'} = \frac{d\sigma_\Lambda^+ - d\sigma_\Lambda^-}{d\sigma_\Lambda^+ + d\sigma_\Lambda^-}, \tag{64}$$

where now the superscripts $^+$ and $^-$ refer to Λ spin projections along and opposite to the $i = z$ or $i = x$ axes, and the incident photon is circularly polarized with positive helicity.

The bulk of recent electroproduction data has been obtained by the Hall C Collaboration and the CLAS Collaboration at Jefferson Lab. Here we fit the most recent results obtained by CLAS [35] for the virtual photoproduction structure functions defined by Eqs. (49). The CLAS Collaboration has also recently obtained data for several electroproduction spin observables [36], but we leave consideration of these data to a future work.

In carrying out the fits, we minimized the χ^2 per degree of freedom defined by the relation

$$\frac{\chi^2}{\nu} = \sum \frac{(Y_{\text{calc}} - Y_{\text{exp}})^2}{\sigma^2}, \tag{65}$$

where the sum is over all of the individual data points, Y_{calc} and Y_{exp} are the calculated and experimental values of the

observable, and σ^2 is the squared statistical uncertainty in Y_{exp}. The number of degrees of freedom is given by $\nu = N_{\text{data}} - N_{\text{par}}$, where N_{data} is the number of data points and N_{par} is the number of parameters in the fit.

Because the number of parameters to be fit is rather large, it was not feasible to fit all the parameters in a single fitting run. Therefore, we employed an iterative procedure in which only a subset of all the model parameters was fit in each run. As mentioned in the introduction, due to a sign error in the t-channel Born term, it was necessary to refit the photoproduction data considered in Ref. [32]. Using the photoproduction parameters from the resulting fit, we next fit the form-factor parameters to the electroproduction data. Then, using these form-factor parameters, we refit the photoproduction parameters simultaneously to the photoproduction and electroproduction data. Using the new set of photoproduction parameters, the form-factor parameters were then refit to the electroproduction data. We found that this iterative scheme converges quite well after only two iterations. To obtain a good fit to the data, we tried varying the starting parameters but did not significantly improve our initial fit.
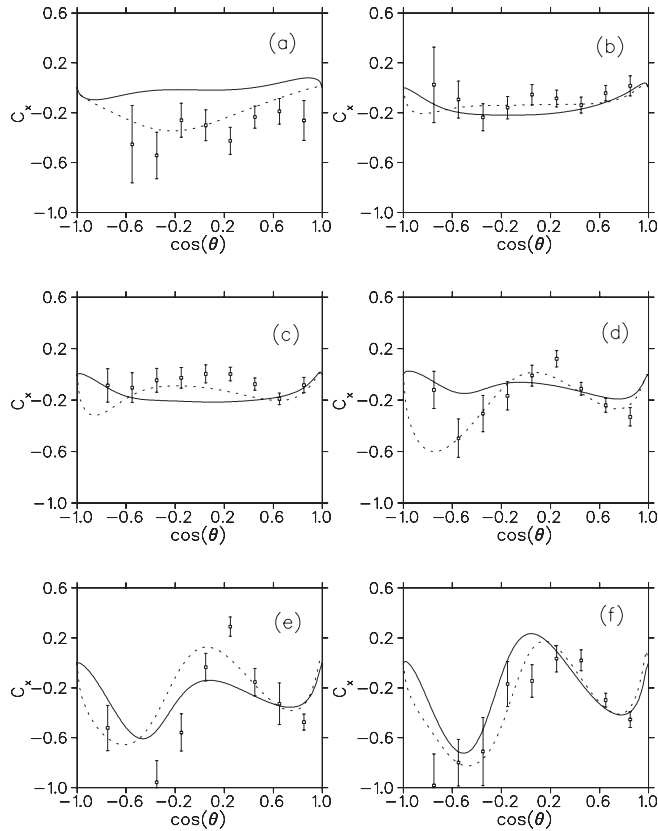
FIG. 4. C_x vs. $\cos(\theta)$ for (a) $W = 1.734$ GeV, (b) $W = 1.839$ GeV, (c) $W = 1.939$ GeV, (d) $W = 2.035$ GeV, (e) $W = 2.126$ GeV, and (f) $W = 2.212$ GeV, where θ is the c.m. scattering angle and W is the c.m. energy. The solid curve was obtained by fitting both photoproduction and electroproduction data, the dashed curve by fitting just the photoproduction data. Data are from Ref. [31].

FIG. 5. C_z vs. $\cos(\theta)$ for (a) $W = 1.734$ GeV, (b) $W = 1.839$ GeV, (c) $W = 1.939$ GeV, (d) $W = 2.035$ GeV, (e) $W = 2.126$ GeV, and (f) $W = 2.212$ GeV, where θ is the c.m. scattering angle and W is the c.m. energy. The solid curve was obtained by fitting both photoproduction and electroproduction data, the dashed curve by fitting just the photoproduction data. Data are from Ref. [31].

VI. NUMERICAL RESULTS AND DISCUSSION

The photoproduction parameters obtained from the simultaneous fit of photoproduction and electroproduction data are presented in Table II. This table lists the fit values of all the coupling strength products defined in Sec. II. For comparison, we have also listed the corresponding parameter values obtained by fitting the photoproduction data alone. As noted in Sec. II, the widths of the high-mass nucleon resonances were not refit in the present study; instead, the width values reported in Ref. [32] were employed.

Even a cursory examination of the numbers in Table II reveals that the two parameters sets are quite different. This indicates that photoproduction data alone are not sufficient to uniquely constrain the coupling parameters associated with effective Lagrangian treatments of electromagnetic strangeness production. The longitudinal degrees of freedom associated with the virtual photons exchanged in electroproduction appear to be crucial, not only in fixing electromagnetic form factors, but also in fixing the underlying strangeness production mechanism itself.

The quality of our fits is illustrated in Figs. 2–6. These five figures display the photoproduction observables defined by Eqs. (61)–(64) as functions of $\cos(\theta)$, where θ is the c.m.
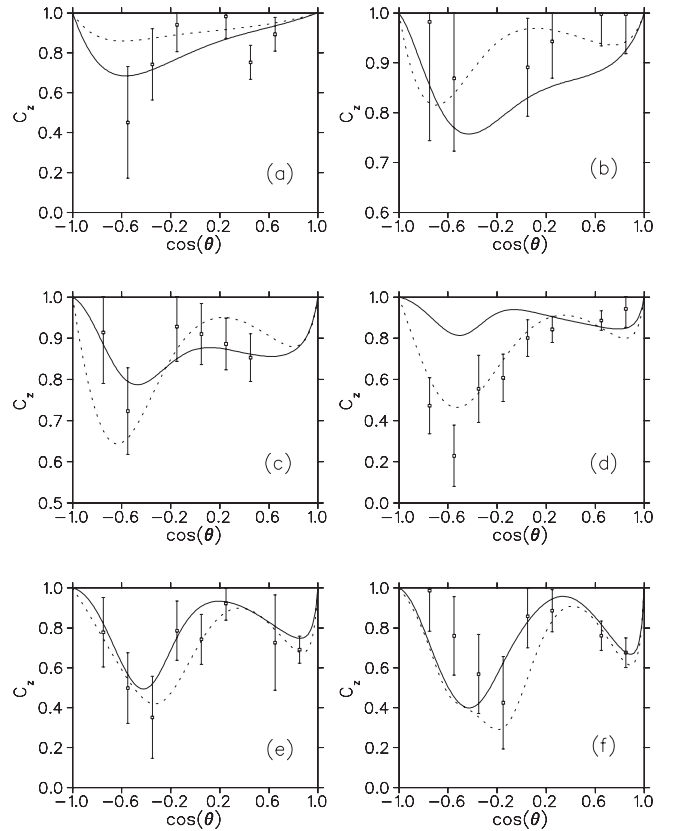
scattering angle, for several values of the c.m. energy W. In each of these figures, the solid and dashed curves correspond respectively to the fit obtained with both photoproduction and electroproduction data and to the fit obtained with the photoproduction data alone.

As seen in Fig. 2, the two fits yield comparable results for the differential cross section. The fits differ mainly at very forward angles and at extreme backward angles. Overall, both fits, despite the differences in the fit parameters, provide a quantitatively good account of the differential cross section.

The two fits differ more substantially in the results obtained for the polarization observables. The relative quality of the two fits depends on both the observable examined and the c.m. energy considered, but overall the qualities of the two fits are comparable. For the hyperon polarization asymmetry (Fig. 3), the dotted curves generally do a little better than the solid curves at the lower energies. At 2.228 GeV, however, the solid fit is consistent with the data near $\cos(\theta) = -0.2$, while the dashed curve exhibits a large peak not seen in the data.

For the double polarization observables, C_x and C_z, the dashed curves are somewhat better than the solid curves, especially at lower energies. The contrast between the two curves is especially pronounced at 2.035 GeV, where the dashed curve generally reproduces the angular distribution of
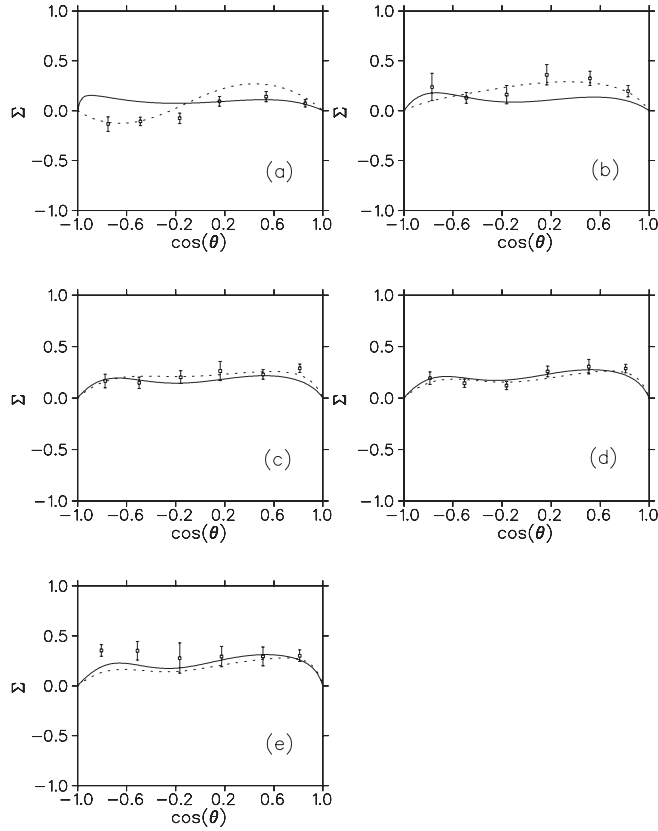
FIG. 6. Photon beam asymmetry vs. $\cos(\theta)$ for (a) $W = 1.702$ GeV, (b) $W = 1.754$ GeV, (c) $W = 1.808$ GeV, (d) $W = 1.859$ GeV, and (e) $W = 1.906$ GeV, where θ is the c.m. scattering angle and W is the c.m. energy. The solid curve was obtained by fitting both photoproduction and electroproduction data, the dashed curve by fitting just the photoproduction data. Data are from Ref. [26].

TABLE III. Fit results for the electromagnetic form factor parameters.

	Λ	α
Spin $-\frac{1}{2}$ resonances		
$N(1440)$	1.4572	2.8997
$N(1535)$	1.6180	4.5155
$N(1650)$	4.6512	-4.8632
$N(1710)$	2.6098	4.0269
$F_1(\Lambda)$	1.4653	0.7876
$F_2(\Lambda)$	4.7441	-1.4324
$\Lambda(1405)$	2.8688	-0.4031
$\Lambda(1670)$	0.2707	-0.5281
Σ	1.8314	-0.8612
Spin-$\frac{3}{2}$ resonances		
$N(1520)$	1.7213	3.4965
$N(1700)$	3.7186	-3.8566
$N(1720)$	1.5354	3.7758
$N(1900)$	4.6720	-1.3748
$N(2080)$	4.2171	2.6698
$\Lambda(1890)$	0.4491	-0.0360
$\Sigma(1385)$	0.7034	4.0338
$\Sigma(1940)$	0.2584	2.3431
Spin-$\frac{5}{2}$ resonances		
$N(1675)$	1.1856	4.8271
$N(1680)$	1.1045	1.0577
$N(2000)$	1.4616	3.6176
$N(2200)$	3.3698	-2.8773
$\Lambda(1820)$	1.1050	2.4088
$\Lambda(1830)$	0.2133	1.6144
$\Lambda(2110)$	0.5460	-0.4098
$\Sigma(1775)$	0.2576	3.0308
$\Sigma(1915)$	1.0454	1.6727
t-channel resonances		
	Λ_{K^*}	
$K(892)$	0.211	
$K(1270)$	0.672	

the data, while the solid curve is too flat. It should be noted that, for the observable C_z, the error bars in the data are so large as to preclude any definite conclusions as to the quality of the fits.

For the photon beam asymmetry, the two fits yield curves that are quite close together. Once again, the dashed curve seems to be better at lower energies. At the higher energies, both curves fit the data quite well. Figure 6 displays results for energies up to 1.906 GeV. Higher-energy data exist but are limited to forward angles. Although not shown in the figure, the higher-energy data were included in the fit.

The electromagnetic form factor parameters obtained by fitting the electroproduction data are listed in Table III. For the ground-state hyperons and the baryon resonances, the second and third columns give the fit values for the form-factor mass parameter Λ and coupling parameter α defined in Eq. (54). For the kaon resonances, the second column lists the fit values of the form factor mass defined in Eq. (53). Note that, for the ground-state Λ (the u channel Born term), the charge and magnetic form factors are related to F_1 and F_2 through Eqs. (55) and (56).

We have not listed parameter uncertainties for these values as the iterative fitting procedure described in the previous section makes the interpretation of these uncertainties unclear. The nominal uncertainties associated with the form-factor segment of the iterative procedure (generated from the corresponding covariance matrix) suggest that there exist significant correlations among the u-channel form-factor parameters. This is consistent with the results of Ref. [32], where significant correlations among the u-channel coupling parameters were noted.

The quality of our electroproduction fits is illustrated in Figs. 7–13. The first three figures exhibit the energy dependences of the structure functions σ_U, σ_{TT}, and σ_{LT}, defined by Eqs. (49) and (51), for three different kaon scattering angles and two different values of the squared virtual-photon 4-momentum. The first figure reveals that, while the fit to σ_U generally follows the energy dependence of the data, there are significant discrepancies within certain energy ranges. In particular, at the lower $-q^2$ value, the fit lies below the data between 1.72 and 1.85 GeV, while at the higher $-q^2$ value, the fit lies above the data at energies exceeding 2.22 GeV.
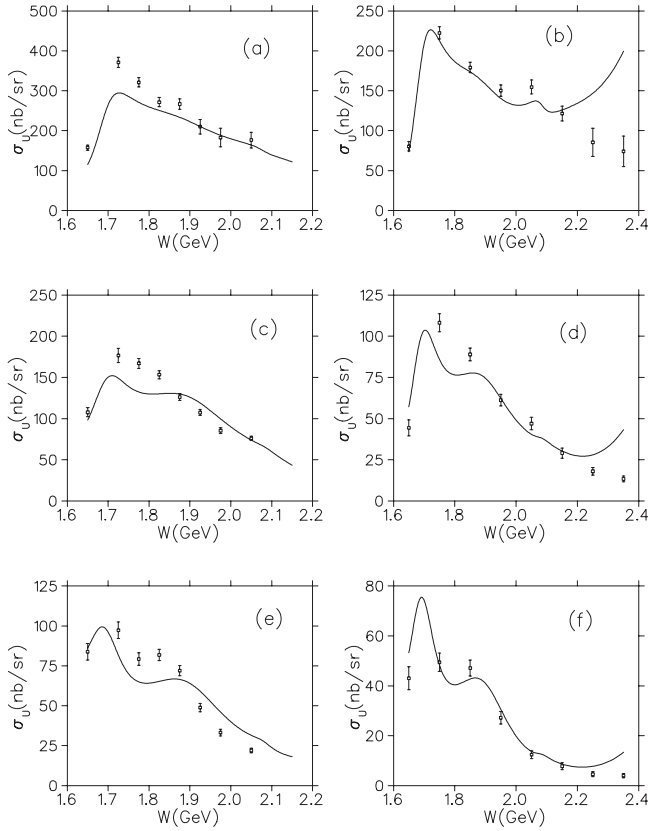
FIG. 7. σ_U vs. W for (a) $\cos(\theta) = 0.90$ and $-q^2 = 0.65$ GeV^2, (b) $\cos(\theta) = 0.90$ and $-q^2 = 1.55$ GeV^2, (c) $\cos(\theta) = 0.35$ and $-q^2 = 0.65$ GeV^2, (d) $\cos(\theta) = 0.35$ and $-q^2 = 1.55$ GeV^2, (e) $\cos(\theta) = -0.25$ and $-q^2 = 0.65$ GeV^2, and (f) $\cos(\theta) = -0.25$ and $-q^2 = 1.55$ GeV^2, where θ and W are the scattering angle and energy in the $K\Lambda$ c.m. frame, and q^2 is the square of the virtual-photon 4-momentum. The $-q^2 = 0.65$ GeV^2 results were obtained with $E = 2.567$ GeV and the $-q^2 = 1.55$ GeV^2 results with $E = 4.056$ GeV, where E is the energy of the incident electron in the laboratory frame. Data are from Ref. [35].

The fits to σ_{TT} and σ_{LT} are generally of lower quality than the fit to σ_U. For both observables the fits are better at the higher $-q^2$ value and at more backward angles. At the forward angle, the data for σ_{TT} exhibit more structure than is seen in the fit, which is quite flat at that angle. At the other two angles, the fit to σ_{TT} is pretty good at the higher $-q^2$ value but lies above the data at the lower $-q^2$ value for energies below 1.9 GeV. Similar observations apply to the σ_{LT} fit: it misses the energy dependence of the data at the forward angle, and at the other angles reproduces the data much better at the higher $-q^2$ value than the lower value.

Figures 10–12 display the angular distributions of the same three structure functions for selected energies and squared photon 4-momentum. Again, it can be seen that the fit to σ_U is much better than the fits to σ_{TT} and σ_{LT}. Also, as seen in the earlier figures, the fits to σ_{TT} and σ_{LT} generally tend not to reproduce the data at forward angles, especially at the lowest energy value.

As mentioned earlier, the CLAS data for the two structure functions σ_T and σ_L are quite limited. Except for just a few
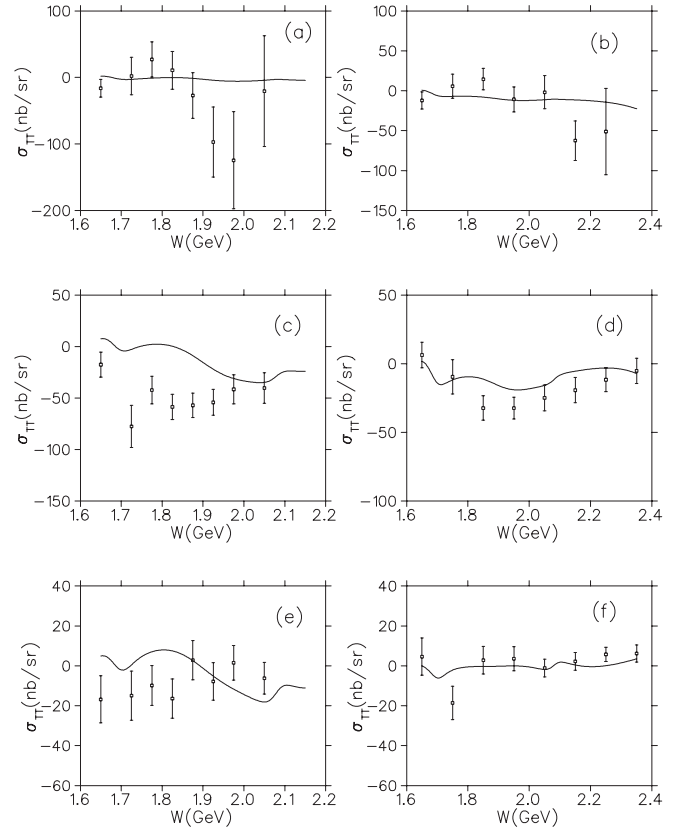

FIG. 8. σ_{TT} vs. W for the same values of $\cos(\theta)$ and $-q^2$ as in Fig. 7, where θ and W are the scattering angle and energy in the $K\Lambda$ c.m. frame, and q^2 is the square of the virtual photon 4-momentum. Data are from Ref. [35].

points, data for these structure functions exist for just $-q^2 = 1.0$ GeV^2 and for energies between 1.75 and 1.95 GeV. For this reason, we present only angular distributions for σ_T and σ_L at the single q^2 for which data exists. These are exhibited in Fig. 12 for three different energy values, with the σ_T fits on the left and the σ_L fits on the right. As can be seen in the figure, the fits at the highest energy value are reasonably good, but the fits at the lowest energy diverge from the data significantly at forward angles. More data for different values of q^2 would certainly be useful here.

In summary, we have presented a new fit of recent kaon photoproduction and electroproduction data from a variety of sources using an effective Lagrangian model supplemented with electromagnetic form factors. We included photoproduction data from threshold up to a c.m. energy of 2.3 GeV and CLAS electroproduction data for a variety of ΣK c.m. energies and virtual-photon 4-momenta.

Overall, the new fit yields good representations of both the photoproduction data and the electroproduction data. When compared with a fit to photoproduction data alone, the fit presented here, while yielding quite different coupling parameters, nevertheless describes the photoproduction data with a comparable level of precision. This indicates that photoproduction data alone are not adequate to uniquely constrain effective Lagrangian models of electromagnetic strangeness production.
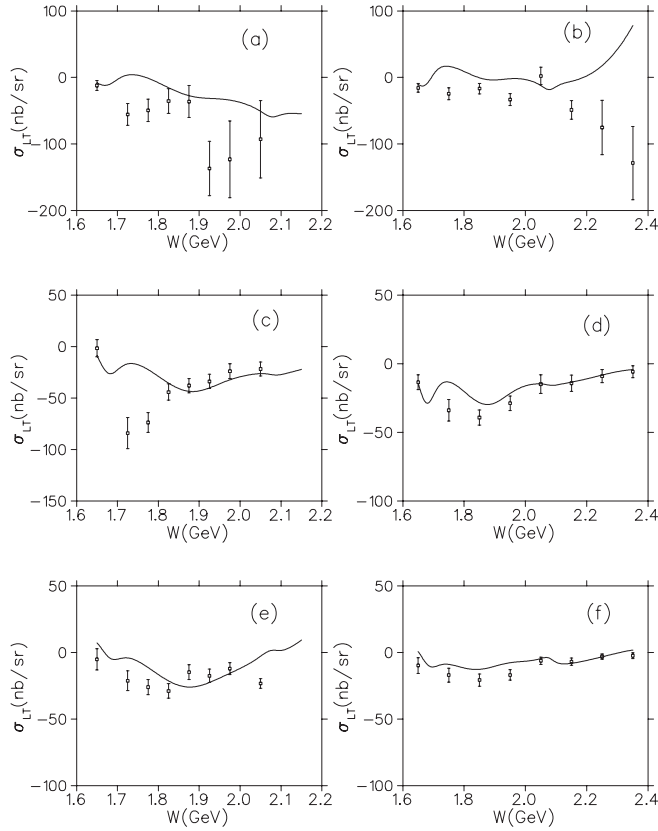
FIG. 9. σ_{LT} vs. W for the same values of $\cos(\theta)$ and $-q^2$ as in Fig. 7, where θ and W are the scattering angle and energy in the $K\Lambda$ c.m. frame, and q^2 is the square of the virtual photon 4-momentum. Data are from Ref. [35].

To achieve a good fit to the CLAS electroproduction data, it was necessary to include the ground-state hyperon form factors among the fitted parameters. If we simply set these form factors equal to the neutron form factors, we cannot achieve even a semiquantitative fit of the data. In general, our fit to the electroproduction data is reasonably good, although not as good as the photoproduction fit.

APPENDIX: AMPLITUDE OPERATORS

Here we list the various α, β, and D operators that appear in Eqs. (46) and (47) for the hadronic current matrix elements. All expressions are given without form factors except for the Born charge contributions. Since the form factors are intimately connected with the counter terms in these contributions, they have been given with the form factors included.
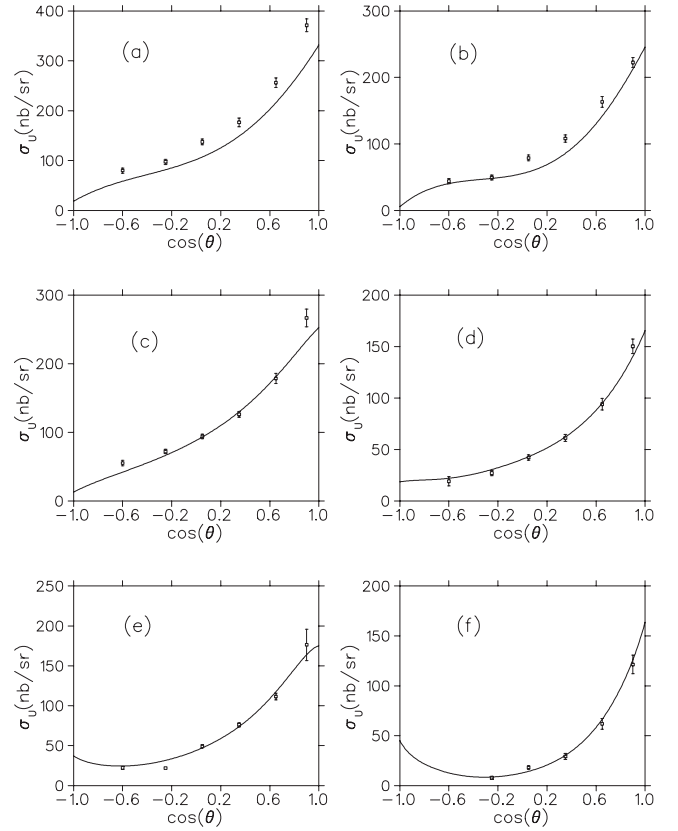

FIG. 10. σ_U vs. $\cos(\theta)$ (a) $W = 1.725$ GeV and $-q^2 = 0.65$ GeV^2, (b) $W = 1.750$ GeV and $-q^2 = 1.55$ GeV^2, (c) $W = 1.875$ GeV and $-q^2 = 0.65$ GeV^2, (d) $W = 1.950$ GeV and $-q^2 = 1.55$ GeV^2, (e) $W = 2.050$ GeV and $-q^2 = 0.65$ GeV^2, and (f) $W = 2.150$ GeV and $-q^2 = 1.55$ GeV^2, where θ and W are the scattering angle and energy in the $K\Lambda$ c.m. frame, and q^2 is the square of the virtual photon 4-momentum. The $-q^2 = 0.65$ GeV^2 results were obtained with $E = 2.567$ GeV and the $-q^2 = 1.55$ GeV^2 results with $E = 4.056$ GeV, where E is the energy of the incident electron in the laboratory frame. Data are from Ref. [35].

In the t channel for an intermediate ground-state kaon, the only nonzero operator is the α_2 operator given by

$$\alpha_2 = \frac{eg_{\Lambda Kp}}{p_I^2 - m_K^2} F_K(q^2)(2\mathbf{p_K} - \mathbf{q})$$
$$+ [1 - F_K(q^2)] \left(\frac{2p_K \cdot q}{q^2} - 1 \right) \mathbf{q}, \quad (A1)$$

where p_I is the 4-momentum of the intermediate kaon, $\mathbf{q}$ is the 3-momentum of the virtual photon, and $F_K(q^2)$ is the kaon electromagnetic form factor.

For the other t-channel contributions, we define products of the coupling strengths and energy denominators:

$$G_V = \frac{G_{K^\star}^V}{m_{sc}} \frac{1}{p_R^2 - m_R^2},$$
$$G_T = \frac{G_{K^\star}^T}{m_{sc}(m_\Lambda + m_p)} \frac{1}{p_R^2 - m_R^2}, \quad (A2)$$

where $G_{K^\star}^V$ and $G_{K^\star}^T$ are the t-channel coupling products given by Eqs. (32), m_{sc} is the kaon resonance scaling mass appearing
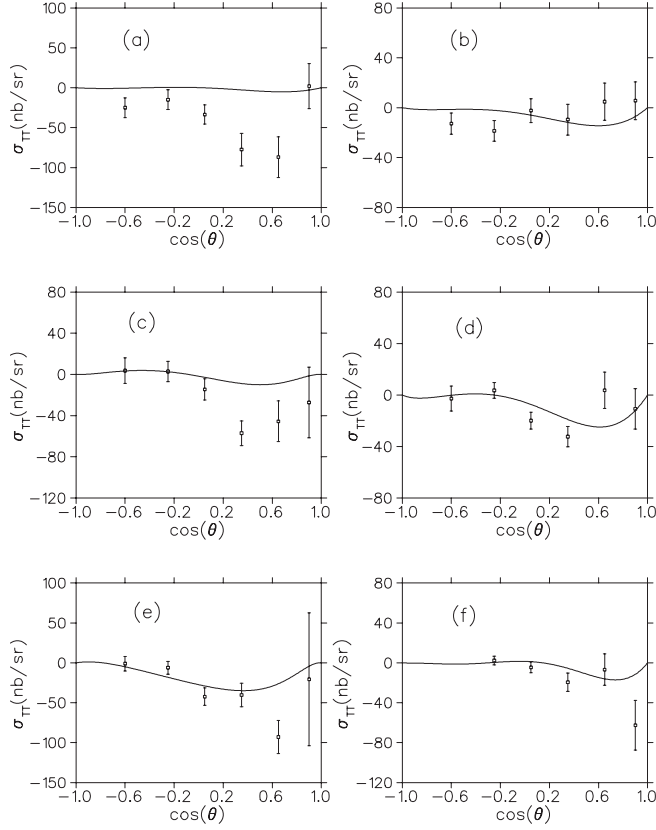
FIG. 11. σ_{TT} vs. $\cos(\theta)$ for the same values of W and $-q^2$ as in Fig. 10, where θ and W are the scattering angle and energy in the $K\Lambda$ c.m. frame, and q^2 is the square of the virtual photon 4-momentum. Data are from Ref. [35].
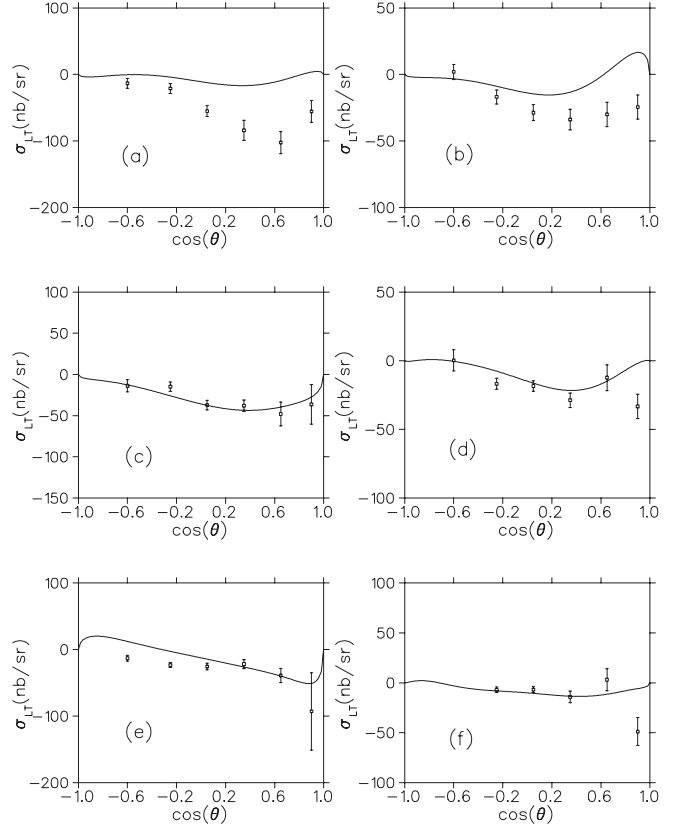

FIG. 12. σ_{LT} vs. $\cos(\theta)$ for the same values of W and $-q^2$ as in Fig. 10, where θ and W are the scattering angle and energy in the $K\Lambda$ c.m. frame, and q^2 is the square of the virtual photon 4-momentum. Data are from Ref. [35].

in Eqs. (6), and (8), and p_R and m_R are the 4-momentum and mass of the intermediate kaon resonance. In terms of these products, we obtain

$$
\begin{aligned}
\alpha_1 &= G_T E_R(\mathbf{q} \times \mathbf{p_K}), \quad \alpha_2 = -G_T \sigma \cdot \mathbf{p_R}(\mathbf{q} \times \mathbf{p_K}), \\
\alpha_3 &= G_V(\mathbf{q} \times \mathbf{p_K}), \quad \alpha_4 = 0, \\
\beta_1 &= -G_V(E_K \mathbf{q} - q_0 \mathbf{p_K}), \quad \beta_2 = 0, \\
\beta_3 &= -G_T E_R(E_K \mathbf{q} - q_0 \mathbf{p_K}), \\
\beta_4 &= -G_T \sigma \cdot \mathbf{p_R}(E_K \mathbf{q} - q_0 \mathbf{p_K})
\end{aligned} \tag{A3}
$$

for an intermediate $K^\star(892)$ resonance and

$$
\begin{aligned}
\alpha_1 &= -G_T \Omega_2(p_R, q)\mathbf{p_R}, \quad \alpha_2 = -G_T \Sigma_2(p_R, q)\mathbf{p_R}, \\
\alpha_3 &= G_V \sigma \cdot \mathbf{q}\mathbf{p_R}, \quad \alpha_4 = -G_V q_0 \mathbf{p_R}, \quad D_1 = 0, \\
D_2 &= G_V p_R \cdot q, \quad D_3 = G_T \sigma \cdot \mathbf{p_R} p_R \cdot q, \\
D_4 &= G_T E_R p_R \cdot q
\end{aligned} \tag{A4}
$$

for an intermediate $K^\star(1270)$ resonance, where the operators Σ_2 and Ω_2 are defined by the relations

$$
\begin{aligned}
\Sigma_2(a, b) &= a_0 b_0 - \sigma \cdot \mathbf{a}\sigma \cdot \mathbf{b}, \\
\Omega_2(a, b) &= b_0 \sigma \cdot \mathbf{a} - a_0 \sigma \cdot \mathbf{b}.
\end{aligned} \tag{A5}
$$

In the s and u-channels, the intermediate baryon can have spin $\frac{1}{2}$, $\frac{3}{2}$, or $\frac{5}{2}$. For spin-$\frac{1}{2}$ baryons we define the quantities

$$
\begin{aligned}
F_{\text{sch}} &= \frac{eg_{\Lambda Kp}}{p_I^2 - m_p^2}, \quad F_{\text{uch}} = \frac{eg_{\Lambda Kp}}{p_I^2 - m_\Lambda^2}, \\
F_s &= \frac{F_{N^\star}}{2m_p} D_s(p_R), \quad F_u = \frac{F_{Y^\star}}{2m_\Lambda} D_u(p_R),
\end{aligned} \tag{A6}
$$

where p_I is the 4-momentum of the intermediate proton or Λ in the charge terms, $F_{N^\star}$ and $F_{Y^\star}$ ($Y = \Lambda$ or Σ) are the coupling products given by Eqs. (29), and the energy denominators are defined by

$$
\begin{aligned}
D_s(p_R) &= \left(p_R^2 - m_R^2 + im_R\Gamma_R\right)^{-1}, \\
D_u(p_R) &= \left(p_R^2 - m_R^2\right)^{-1}.
\end{aligned} \tag{A7}
$$

The s-channel positive-parity spin-$\frac{1}{2}$ operators are then given by

$$
\begin{aligned}
\alpha_1 &= 0, \quad \alpha_2 = -F_s m_R \mathbf{q}, \quad \alpha_3 = -F_s \sigma \cdot \mathbf{p_R}\mathbf{q}, \\
\alpha_4 &= F_s E_R \mathbf{q}, \quad D_1 = F_s \Omega_2(p_R, q), \quad D_2 = -F_s \Sigma_2(p_R, q), \\
D_3 &= F_s m_R \sigma \cdot \mathbf{q}, \quad D_4 = F_s m_R q_0.
\end{aligned} \tag{A8}
$$
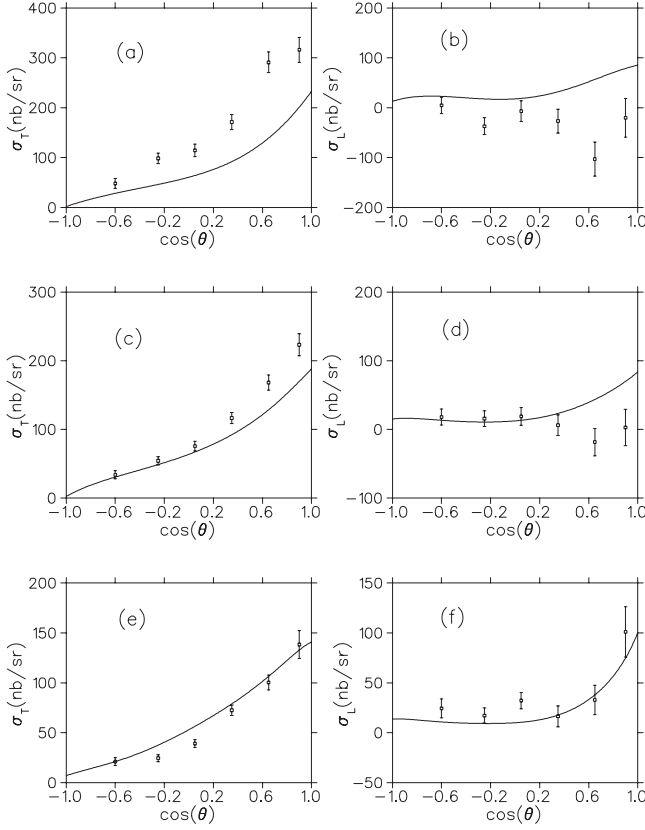
FIG. 13. σ_T vs. $\cos(\theta)$ (left side panels) and σ_L vs. $\cos(\theta)$ (right side panels) for $-q^2 = 1.0$ GeV^2 and $W = 1.750$ GeV [panels (a) and (b)], $W = 1.850$ GeV [panels (c) and (d)], and $W = 1.950$ GeV [panels (e) and (f)], where θ and W are the scattering angle and energy in the $K\Lambda$ c.m. frame, and q^2 is the square of the virtual photon 4-momentum. Data are from Ref. [35].

For the u-channel positive-parity spin-$\frac{1}{2}$ operators, we obtain

$$\alpha_1 = 0, \quad \alpha_2 = -F_u m_R \mathbf{q}, \quad \alpha_3 = F_u[\sigma \cdot \mathbf{p_R q} - 2\sigma \cdot \mathbf{q p_R}],$$

$$\alpha_4 = F_u[-E_R \mathbf{q} + 2q_0 \mathbf{p_R}], \quad D_1 = F_u \Omega_2(q, p_R),$$
$$D_2 = -F_u \Sigma_2(q, p_R), \quad D_3 = F_u m_R \sigma \cdot \mathbf{q}, \quad D_4 = F_u m_R q_0. \tag{A9}$$

All of the α operators associated with the charge contributions to the $s-$ and u-channel Born terms are zero except for α_2. After making use of the Dirac equation, the α_2 operator and the D operators are given by

$$D_1 = 0, \quad D_2 = 0, \quad D_3 = F_C(q^2)F_{\text{sch}}\sigma \cdot \mathbf{q},$$
$$D_4 = F_C(q^2)F_{\text{sch}}q_0, \tag{A10}$$
$$\alpha_2 = 2F_C(q^2)F_{\text{sch}}\mathbf{p_p} + eg_{\Lambda Kp}[1 - F_C(q^2)]\frac{\mathbf{q}}{q^2}$$

for the proton charge term and

$$D_1 = 0, \quad D_2 = 0, \quad D_3 = F_C(q^2)F_{\text{uch}}\sigma \cdot \mathbf{q},$$
$$D_4 = F_C(q^2)F_{\text{uch}}q_0, \tag{A11}$$
$$\alpha_2 = F_C(q^2)\left[2F_{\text{uch}}(\mathbf{p_\Lambda} - \mathbf{q}) + eg_{\Lambda Kp}\frac{\mathbf{q}}{q^2}\right]$$

for the Λ charge term, where $F_C(q^2)$ is the proton or Λ charge form factor.

The spin-$\frac{3}{2}$ and spin- resonance contributions in the s and u channels each involve two coupling products. For the spin-$\frac{3}{2}$ contributions we define the combinations

$$G_{s1} = \frac{G_{N^\star}^1}{m_\pi 2m_p}D_s(p_R), \quad G_{s2} = \frac{G_{N^\star}^2}{m_\pi (2m_p)^2}D_s(p_R),$$

$$G_{u1} = \frac{G_{Y^\star}^1}{m_\pi 2m_\Lambda}D_u(p_R), \quad G_{u2} = \frac{G_{Y^\star}^2}{m_\pi (2m_\Lambda)^2}D_u(p_R), \tag{A12}$$

with $G_{N^\star}^1$, $G_{N^\star}^2$, $G_{Y^\star}^1$, and $G_{Y^\star}^2$ given by Eqs. (30). The corresponding combinations for spin $\frac{5}{2}$ just have the denominator factors of m_π replaced by factors of m_π^3.

In the s channel the positive-parity spin-$\frac{3}{2}$ operators are then given by

$$\alpha_1 = G_{s1}\left[-\Omega_2(p_R, q)\mathbf{k} + \frac{1}{3}\Omega_2(p_K, q)\mathbf{p_R} + \frac{2}{3}\Omega_2(p_R, p_K)\mathbf{q}\right]$$
$$+ \frac{1}{3}G_{s2}m_R[-\beta_p\Omega_2(p_R, p_K)\mathbf{p_R} - \Omega_2(p_R, y)\mathbf{p_p} + \Omega_2(p_K, q)\mathbf{p_p}],$$

$$\alpha_2 = G_{s1}\left[-\Sigma_2(p_R, q)\mathbf{k} + \frac{1}{3}\Sigma_2(p_K, q)\mathbf{p_R} + \frac{2}{3}\Sigma_2(p_R, p_K)\mathbf{q} - \frac{2}{3}\alpha_K m_R^2\mathbf{q}\right]$$
$$+ G_{s2}m_R^3\mathbf{b} + \frac{1}{3}G_{s2}m_R[-\beta_p\Sigma_2(p_R, p_K)\mathbf{p_R} - \Sigma_2(p_R, y)\mathbf{p_p} + \Sigma_2(p_K, q)\mathbf{p_p}],$$

$$\alpha_3 = G_{s1}\left[m_R\sigma \cdot \mathbf{qk} + \frac{2}{3}m_R(\alpha_K\sigma \cdot \mathbf{p_R} - \sigma \cdot \mathbf{k})\mathbf{q} + \frac{1}{3}\Omega_3(p_R, p_K, q)\frac{\mathbf{p_R}}{m_R}\right]$$
$$+ G_{s2}m_R^2\left[-\sigma \cdot \mathbf{p_R b} + \frac{1}{3}\beta_p\sigma \cdot \mathbf{p_K p_R} + \frac{1}{3}\sigma \cdot \mathbf{y p_p} + \frac{1}{3}\Omega_3(p_R, p_K, q)\frac{\mathbf{p_p}}{m_R^2}\right],$$

$$\alpha_4 = G_{s1}\left[-m_R q_0\mathbf{k} + \frac{2}{3}m_R(E_K - \alpha_K E_R)\mathbf{q} + \frac{1}{3}\Sigma_3(p_R, p_K, q)\frac{\mathbf{p_R}}{m_R}\right]$$
$$+ G_{s2}m_R^2\left[E_R\mathbf{b} - \frac{1}{3}\beta_p E_K\mathbf{p_R} - \frac{1}{3}y_0\mathbf{p_p} + \frac{1}{3}\Sigma_3(p_R, p_K, q)\frac{\mathbf{p_p}}{m_R^2}\right],$$

$$D_1 = \frac{1}{3}G_{s1}m_R[2\Omega_2(p_K,q) - \Omega_2(p_R,y) - \alpha_K\Omega_2(p_R,q)] + \frac{1}{3}G_{s2}m_R^2\beta_p\Omega_2(p_R,p_K),$$

$$D_2 = \frac{1}{3}G_{s1}m_R\big[\Sigma_2(p_R,y) + \alpha_K\Sigma_2(p_R,q) - 2\Sigma_2(p_K,q) + 3m_R^2\beta_K\big] + \frac{1}{3}G_{s2}m_R^2\big[-\beta_p\Sigma_2(p_R,p_K) + \alpha_K\beta_p m_R^2\big],$$

$$D_3 = \frac{1}{3}G_{s1}\big[m_R^2(3\beta_K\sigma\cdot\mathbf{p_R} + \sigma\cdot\mathbf{y} + \alpha_K\sigma\cdot\mathbf{q}) + 2\Omega_3(p_R,p_K,q)\big] + \frac{1}{3}G_{s2}m_R^3\beta_p(\alpha_K\sigma\cdot\mathbf{p_R} - \sigma\cdot\mathbf{p_K}),$$

$$D_4 = \frac{1}{3}G_{s1}\big[m_R^2(3\beta_K E_R + E_y + \alpha_K q_0) - 2\Sigma_3(p_R,p_K,q)\big] + \frac{1}{3}G_{s2}m_R^3\beta_p(\alpha_K E_R - E_K) \tag{A13}$$

with

$$\alpha_q = \frac{p_R\cdot q}{m_R^2}, \quad \alpha_K = \frac{p_R\cdot p_K}{m_R^2}, \quad \beta_p = \frac{p_p\cdot q}{m_R^2}, \quad \beta_K = \frac{q\cdot k}{m_R^2}, \quad k = p_K - \frac{2}{3}\alpha_K p_R, \quad y = \alpha_K q - \alpha_q p_K, \quad b = \beta_p k - \beta_K p_p. \tag{A14}$$

The operators $\Sigma_3(a,b,c)$ and $\Omega_3(a,b,c)$ are defined by the relations

$$\Sigma_3(a,b,c) = a_0\Sigma_2(b,c) - \sigma\cdot\mathbf{a}\Omega_2(b,c), \quad \Omega_3(a,b,c) = a_0\Omega_2(b,c) - \sigma\cdot\mathbf{a}\Sigma_2(b,c). \tag{A15}$$

To specify the positve-parity spin-$\frac{3}{2}$ operators in the u channel, we first define the combinations

$$\mathbf{c_1} = \beta_\Lambda\left(\mathbf{k} - \frac{2}{3}\mathbf{p_K}\right) - \beta_K\mathbf{p_\Lambda}, \quad \mathbf{c_2} = \frac{1}{3}\left(\frac{q^2}{m_R^2}\mathbf{p_\Lambda} - \beta_\Lambda\mathbf{q}\right), \quad \mathbf{c_3} = 2\beta_K\mathbf{p_R} - \frac{2}{3}\alpha_K\mathbf{q}2\alpha_q(\mathbf{p_K} - \mathbf{k}),$$

$$\mathbf{c_4} = \frac{4}{3}\mathbf{p_K} - \frac{2}{3}\alpha_K\mathbf{p_R} - \mathbf{k}, \quad \mathbf{c_5} = \mathbf{k} - \frac{4}{3}\mathbf{p_K}, \tag{A16}$$

with

$$\beta_\Lambda = \frac{p_\Lambda\cdot q}{m_R^2} \tag{A17}$$

and the other parameters as defined above. Then the positive-parity spin-$\frac{3}{2}$ operators in the u channel are given by

$$\alpha_1 = G_{u2}m_R\left[\Omega_2(p_R,p_K)\mathbf{c_2} + \frac{1}{3}[\alpha_K\Omega_2(p_R,q) + \Omega_2(q,p_K)]\mathbf{p_\Lambda}\right]$$
$$+ G_{u1}\left[-\Omega_2(q,p_K)\mathbf{p_R} + \frac{2}{3}\Omega_2(p_R,p_K)\mathbf{q} + \Omega_2(p_R,q)\mathbf{c_5}\right],$$

$$\alpha_2 = G_{u2}m_R\left[\Sigma_2(p_R,p_K)\mathbf{c_2} + \frac{1}{3}[\alpha_K\Sigma_2(p_R,q) + \Sigma_2(q,p_K)]\mathbf{p_\Lambda} + m_R^2\mathbf{c_1}\right]$$
$$+ G_{u1}\left[-\Sigma_2(q,p_K)\mathbf{p_R} + \frac{2}{3}\Sigma_2(p_R,p_K)\mathbf{q} + \Sigma_2(p_R,q)\mathbf{c_5} + m_R^2\mathbf{c_3}\right],$$

$$\alpha_3 = G_{u2}m_R^2\left[\sigma\cdot\mathbf{p_R}\mathbf{c_1} + \sigma\cdot\mathbf{p_K}\mathbf{c_2} + \frac{1}{3}\left(\alpha_K\sigma\cdot\mathbf{q} - \frac{1}{m_R^2}\Omega_3(p_R,q,p_K)\right)\mathbf{p_\Lambda}\right] \tag{A18}$$
$$+ \frac{1}{3}G_{u1}m_R\left[3\sigma\cdot\mathbf{q}\mathbf{c_4} - 2\sigma\cdot\mathbf{p_K}\mathbf{q} + 2\sigma\cdot\mathbf{p_R}\mathbf{y} - \frac{1}{m_R^2}\Omega_3(p_R,q,p_K)\mathbf{p_R}\right],$$

$$\alpha_4 = -G_{u2}m_R^2\left[E_R\mathbf{c_1} + E_K\mathbf{c_2} + \frac{1}{3}\left(\alpha_K q_0 + \frac{1}{m_R^2}\Sigma_3(p_R,q,p_K)\right)\mathbf{p_\Lambda}\right]$$
$$+ \frac{1}{3}G_{u1}m_R l\left[-3q_0\mathbf{c_4} + 2E_K\mathbf{q} - 2E_R\mathbf{y} - \frac{1}{m_R^2}\Sigma_3(p_R,q,p_K)\mathbf{p_R}\right],$$

$$D_1 = \frac{1}{3}G_{u2}m_R^2\beta_\Lambda\Omega_2(p_R,p_K) + \frac{1}{3}G_{u1}m_R[-2\Omega_2(q,p_K) + \alpha_q\Omega_2(p_R,p_K) - 2\alpha_K\Omega_2(p_R,q)],$$

$$D_2 = \frac{1}{3}G_{u2}m_R^2\big[-\beta_\Lambda\Sigma_2(p_R,p_K) + m_R^2\beta_\Lambda\alpha_K\big] + \frac{1}{3}G_{u1}m_R[2\Sigma_2(q,p_K) - \alpha_q\Sigma_2(p_R,p_K) + 2\alpha_K\Sigma_2(p_R,q) - m_R^2(3\beta_K + 2\alpha_K\alpha_q)],$$

$$D_3 = \frac{1}{3}G_{u2}m_R^3[-\beta_\Lambda\alpha_K\sigma\cdot\mathbf{p_R} + \beta_\Lambda\sigma\cdot\mathbf{p_K}] + \frac{1}{3}G_{u1}m_R^2\left[-3\alpha_q\sigma\cdot\mathbf{p_K} + 2\alpha_K\sigma\cdot\mathbf{q} - 3\beta_K\sigma\cdot\mathbf{p_R} - 2\frac{1}{m_R^2}\Omega_3(p_R,q,p_K)\right],$$

$$D_4 = \frac{1}{3}G_{u2}m_R^3[-\beta_\Lambda\alpha_K E_R + \beta_\Lambda E_K] + \frac{1}{3}G_{u1}m_R^2\left[-3\alpha_q E_K + 2\alpha_K q_0 - 3\beta_K E_R + 2\frac{1}{m_R^2}\Sigma_3(p_R,q,p_K)\right].$$

In connection with the positive-parity spin-$\frac{5}{2}$ nucleon resonances, we define

$$a_K = \frac{1}{5}\left(\alpha_K^2 - \frac{m_K^2}{m_R^2}\right), \quad b_K = \beta_K^2 + \frac{1}{m_R^2}a_K q \cdot z, \quad \mathbf{d_1} = \frac{1}{5}\left(2\beta_K\mathbf{q} + \frac{q^2}{m_R^2}\mathbf{h}\right), \quad \mathbf{d_2} = \frac{1}{5}(\alpha_q\mathbf{h} + \beta_K\mathbf{p_R}),$$

$$\mathbf{d_3} = \beta_K\mathbf{h} + 2\frac{1}{m_R^2}h\cdot p_R\mathbf{d_2} + a_K\mathbf{z}, \quad \mathbf{d_4} = \beta_K(\beta_K\mathbf{p_p} - \beta_p\mathbf{h}) + a_K\left(\frac{1}{m_R^2}z\cdot q\mathbf{p_p} - \beta_p\mathbf{z}\right) - \frac{2}{5}\frac{1}{m_R^2}(\beta_p\beta_K h\cdot p_R\mathbf{p_R}),$$

$$\mathbf{d_5} = \frac{1}{5}(\beta_p\mathbf{h} - 2\beta_K\mathbf{p_p}), \tag{A19}$$

with

$$h = p_K - \alpha_K p_R, \quad z = q - \alpha_q p_R, x \tag{A20}$$

and the α and β parameters defined as for the spin-$\frac{3}{2}$ resonances. The positive-parity spin-$\frac{5}{2}$ s-channel operators are then given by

$$\alpha_1 = G_{s1}m_R^2\left[\Omega_2(p_R, q)\mathbf{d_3} - \Omega_2(p_R, h)\mathbf{d_1} - \frac{p_R^2}{m_R^2}\Omega_2(h, q)\mathbf{d_2}\right] + G_{s2}m_R^3\Omega_2(h, z)\mathbf{d_5},$$

$$\alpha_2 = G_{s1}m_R^2\left[\Sigma_2(p_R, q)\mathbf{d_3} - \Sigma_2(p_R, h)\mathbf{d_1} - \frac{p_R^2}{m_R^2}\Sigma_2(h, q)\mathbf{d_2}\right] + G_{s2}m_R^3\left[\Sigma_2(h, z)\mathbf{d_5} + m_R^2\mathbf{d_4}\right],$$

$$\alpha_3 = G_{s1}m_R^3\left[\sigma\cdot\mathbf{q}\mathbf{d_3} - \sigma\cdot\mathbf{h}\mathbf{d_1} + \frac{1}{m_R^2}\Omega_3(p_R, h, q)\mathbf{d_2}\right] - G_{s2}m_R^2\Omega_3(p_R, h, z)\mathbf{d_5},$$

$$\alpha_4 = G_{s1}m_R^3\left[-q_0\mathbf{d_3} + h_0\mathbf{d_1} + \frac{1}{m_R^2}\Sigma_3(p_R, h, q)\mathbf{d_2}\right] - G_{s2}m_R^2\left[\Sigma_3(p_R, h, z)\mathbf{d_5} + m_R^2E_R\mathbf{d_4}\right], \tag{A21}$$

$$D_1 = \frac{1}{5}G_{s1}m_R^3[2\beta_K\Omega_2(h, z) + \beta_K\Omega_2(h, q)] + \frac{1}{5}G_{s2}m_R^4\beta_K\beta_p\Omega_2(p_R, h),$$

$$D_2 = \frac{1}{5}G_{s1}m_R^3\left[-2\beta_K\Sigma_2(h, z) - \beta_K\Sigma_2(h, q) + 5m_R^2b_K\right] - \frac{1}{5}G_{s2}m_R^4\beta_K\beta_p\Sigma_2(p_R, h),$$

$$D_3 = -\frac{1}{5}G_{s1}m_R^2[2\beta_K\Omega_3(p_R, h, z) + \beta_K\Omega_3(p_R, h, q)] + \frac{1}{5}G_{s2}m_R^5\beta_K\beta_p\sigma\cdot h,$$

$$D_4 = \frac{1}{5}G_{s1}m_R^2[2\beta_K\Sigma_3(p_R, h, z) + \beta_K\Sigma_3(p_R, h, q) - 5m_R^2b_K E_R] + \frac{1}{5}G_{s2}m_R^5\beta_K\beta_p h_0.$$

Finally, in connection with the positive-parity spin-$\frac{5}{2}$ hyperon resonances, we define, in terms of previously defined parameters,

$$\mathbf{b_1} = \beta_k\mathbf{h} + a_K\mathbf{z}, \quad \mathbf{b_2} = \frac{1}{5}(\beta_k\mathbf{p_R} + \alpha_q\mathbf{h}), \quad \mathbf{f_1} = b_K\mathbf{p_\Lambda} - \beta_\Lambda\left(\mathbf{b_1} - \frac{2}{5}\beta_K\mathbf{h}\right), \quad \mathbf{f_2} = \frac{1}{5}(\beta_\Lambda\mathbf{h} - 2\beta_K\mathbf{p_\Lambda}),$$

$$\mathbf{f_3} = \frac{2}{5}\beta_K\alpha_q\mathbf{p_\Lambda} - \beta_\Lambda\mathbf{b_2}, \quad \mathbf{f_4} = -2b_K\mathbf{p_R} - 2a_R\mathbf{h}, \quad \mathbf{f_5} = \mathbf{b_1} - \frac{6}{5}\beta_K\mathbf{h}, \quad \mathbf{f_6} = \frac{4}{5}\beta_K(\mathbf{q} - \alpha_q\mathbf{p_R}) - \frac{1}{5}\frac{q^2}{m_R^2}\mathbf{h}, \tag{A22}$$

$$\mathbf{f_7} = \frac{2}{5}(2\beta_K\mathbf{p_R} - \alpha_q\mathbf{h}) + \frac{p_R^2}{m_R^2}\mathbf{b_2}, \quad \mathbf{f_8} = -\frac{4}{5}\beta_K\mathbf{q} + \frac{1}{5}\frac{q^2}{m_R^2}\mathbf{h}$$

with

$$a_R = -\frac{2}{5}\beta_K\alpha_q\left(2 - \frac{p_R^2}{m_R^2}\right). \tag{A23}$$

Then the positive-parity spin-$\frac{5}{2}$ u-channel operators are given by

$$\alpha_1 = G_{u2}m_R^3[\Omega_2(q, h)\mathbf{f_2} + \Omega_2(p_R, h)\mathbf{f_3}] + G_{u1}m_R^2[\Omega_2(q, h)\mathbf{f_7} + \Omega_2(p_R, h)\mathbf{f_8} + \Omega_2(q, p_R)\mathbf{f_5}],$$

$$\alpha_2 = G_{u2}m_R^3[\Sigma_2(q, h)\mathbf{f_2} + \Sigma_2(p_R, h)\mathbf{f_3} + m_R^2\mathbf{f_1}] + G_{u1}m_R^2[\Sigma_2(q, h)\mathbf{f_7} + \Sigma_2(p_R, h)\mathbf{f_8} + \Sigma_2(q, p_R)\mathbf{f_5} + m_R^2\mathbf{f_4}],$$

$$\alpha_3 = G_{u2}m_R^2[-m_R^2\sigma\cdot\mathbf{p_R}\mathbf{f_1} - p_R^2\sigma\cdot\mathbf{h}\mathbf{f_3} + \Omega_3(p_R, q, h)\mathbf{f_2}]$$

$$- G_{u1}m_R^3\left[\sigma\cdot\mathbf{q}\mathbf{f_5} + \sigma\cdot\mathbf{h}\mathbf{f_6} + \frac{4}{5}\beta_K\alpha_q\sigma\cdot\mathbf{p_R}\mathbf{h} - \frac{1}{m_R^2}\Omega_3(q, p_R, h)\mathbf{b_2}\right],$$

$$\alpha_4 = G_{u2}m_R^2\big[m_R^2 E_R \mathbf{f_1} + p_R^2 h_0 \mathbf{f_3} + \Sigma_3(p_R, q, h)\mathbf{f_2}\big] + G_{u1}m_R^3 \left[q_0\mathbf{f_5} + h_0\mathbf{f_6} + \frac{4}{5}\beta_K\alpha_q E_R\mathbf{h} + \frac{1}{m_R^2}\Sigma_3(q, p_R, h)\mathbf{b_2}\right],$$

$$D_1 = \frac{1}{5}G_{u2}m_R^4\beta_\Lambda\beta_K\Omega_2(p_R, h) + \frac{1}{5}G_{u1}m_R^3[2\beta_K\alpha_q\Omega_2(p_R, h) - 3\beta_K\Omega_2(q, h)],$$

$$D_2 = -\frac{1}{5}G_{u2}m_R^4\beta_\Lambda\beta_K\Sigma_2(p_R, h) + \frac{1}{5}G_{u1}m_R^3\big[-2\beta_K\alpha_q\Sigma_2(p_R, h) + 3\beta_K\Sigma_2(q, h) - 5m_R^2 b_k\big],$$

$$D_3 = -\frac{1}{5}G_{u2}m_R^5\beta_\Lambda\beta_K\sigma\cdot\mathbf{h} + G_{u1}m_R^4\left[a_R\sigma\cdot\mathbf{h} + b_K\sigma\cdot\mathbf{p_R} - \frac{3}{5}\frac{1}{m_R^2}\beta_K\Omega_3(q, p_R, h)\right],$$

$$D_4 = -\frac{1}{5}G_{u2}m_R^5\beta_\Lambda\beta_K h_0 + G_{u1}m_R^4\left[a_R h_0 + b_K E_R + \frac{3}{5}\frac{1}{m_R^2}\beta_K\Sigma_3(q, p_R, h)\right]. \tag{A24}$$

All of the s- and u-channel operator expressions above are for positive-parity resonance contributions to the reaction amplitude. For negative-parity resonances, the α_1, α_2, D_3, and D_4 operators are just the negatives of the corresponding positive-parity operators, while the α_3, α_4, D_1, and D_2 operators are identical to the corresponding positive-parity operators.

---

[1] R. A. Adelseck, C. Bennhold, and L. E. Wright, Phys. Rev. C **32**, 1681 (1985).

[2] R. A. Adelseck and L. E. Wright, Phys. Rev. C **38**, 1965 (1988).

[3] R. A. Adelseck and B. Saghai, Phys. Rev. C **42**, 108 (1990).

[4] R. A. Williams, C.-R. Ji, and S. R. Cotanch, Phys. Rev. C **46**, 1617 (1992).

[5] T. Mart, C. Bennhold, and C. E. Hyde-Wright, Phys. Rev. C **51**, R1074 (1995); H. Haberzettl, C. Bennhold, T. Mart, and T. Feuster, *ibid*. **58**, R40 (1998); H. Haberzettl, C. Bennhold, and T. Mart, Acta Phys. Pol. B **31**, 2387 (2000).

[6] T. Mart and C. Bennhold, Phys. Rev. C **61**, 012201(R) (1999).

[7] H. Haberzettl, C. Bennhold, and T. Mart, Nucl. Phys. A **684**, 475c (2001).

[8] M. K. Cheoun, B. S. Han, B. G. Yu, and I.-T. Cheon, Phys. Rev. C **54**, 1811 (1996); B. S. Han, M. K. Cheoun, K. S. Kim, and I.-T. Cheon, Nucl. Phys. A **691**, 713 (2001).

[9] J. C. David, C. Fayard, G. H. Lamot, and B. Saghai, Phys. Rev. C **53**, 2613 (1996).

[10] T. Mizutani, C. Fayard, G.-H. Lamot, and B. Saghai, Phys. Rev. C **58**, 75 (1998).

[11] S. S. Hsiao, D. H. Lu, and S. N. Yang, Phys. Rev. C **61**, 068201 (2000).

[12] W. T. Chiang, F. Tabakin, T.-S. H. Lee, and B. Saghai, Phys. Lett. B **517**, 101 (2001).

[13] S. Janssen, J. Ryckebusch, W. Van Nespen, D. Debruyne, and T. Van Cauteren, Eur. Phys. J. A **11**, 105 (2001); S. Janssen, J. Ryckebusch, D. Debruyne, and T. Van Cauteren, Phys. Rev. C **65**, 015201 (2001); **66**, 035202 (2002); S. Janssen, D. G. Ireland, and J. Ryckebusch, Phys. Lett. B **562**, 51 (2003).

[14] S. Janssen, J. Ryckebusch, and T. Van Cauteren, Phys. Rev. C **67**, 052201(R) (2003).

[15] O. V. Maxwell, Phys. Rev. C **69**, 034605 (2004).

[16] O. V. Maxwell, Phys. Rev. C **70**, 044612 (2004).

[17] O. V. Maxwell, Phys. Rev. C **76**, 014621 (2007).

[18] A. Usov and O. Scholten, Phys. Rev. C **72**, 025205 (2005).

[19] A. V. Sarantsev, V. A. Nikonov, A. V. Anisovich, E. Klempt, and U. Thoma, Eur. Phys. J. A **25**, 441 (2005); A. V. Anisovich, V. Kleber, E. Klempt, V. A. Nikonov, A. V. Sarantsev, and U. Thoma, *ibid*. **34**, 243 (2007); V. A. Nikonov,

A. V. Anisovich, E. Klempt, A. V. Sarantsev, and U. Thoma, Phys. Lett. B **662**, 245 (2008).

[20] N. Kaiser, T. Waas, and W. Weise, Nucl. Phys. A **612**, 297 (1997).

[21] T. Feuster and U. Mosel, Phys. Rev. C **59**, 460 (1999).

[22] B. Julia-Diaz, B. Saghai, T. S. H. Lee, and F. Tabakin, Phys. Rev. C **73**, 055204 (2006).

[23] B. Borasoy, E. Marco, and S. Wetzel, Phys. Rev. C **66**, 055208 (2002); B. Borasoy, P. C. Bruns, U.-G. Meissner, and R. Nissler, *ibid*. **72**, 065201 (2005); Eur. Phys. J. A **34**, 161 (2007).

[24] M. Q. Tran *et al.*, Phys. Lett. B **445**, 20 (1998); S. Goers *et al.*, *ibid*. **464**, 331 (1999); K. H. Glander *et al.*, Eur. Phys. J. A **19**, 251 (2004).

[25] R. G. T. Zegers *et al.*, Phys. Rev. Lett. **91**, 092001 (2003); M. Sumihama *et al.*, Phys. Rev. C **73**, 035214 (2006).

[26] A. Lleres *et al.*, Eur. Phys. J. A **31**, 79 (2007); A. D'Angelo *et al.*, *ibid*. **31**, 441 (2007).

[27] A. Lleres *et al.*, Eur. Phys. J. A **39**, 149 (2009).

[28] J. W. C. McNabb *et al.*, Phys. Rev. C **69**, 042201 (2004).

[29] D. S. Carman *et al.*, Phys. Rev. Lett. **90**, 131804 (2003); Phys. Rev. C **79**, 065205 (2009).

[30] R. Bradford *et al.*, Phys. Rev. C **73**, 035202 (2006).

[31] R. Bradford *et al.*, Phys. Rev. C **75**, 035205 (2007).

[32] A. de la Puente, O. V. Maxwell, and B. A. Raue, Phys. Rev. C **80**, 065205 (2009).

[33] G. Niculescu *et al.*, Phys. Rev. Lett. **81**, 1805 (1998); L. Teodorescu *et al.*, Nucl. Phys. A **658**, 362 (1999); R. M. Mohring *et al.*, Phys. Rev. C **67**, 055205 (2003).

[34] D. S. Carman *et al.*, Phys. Rev. Lett. **90**, 131804 (2003).

[35] P. Ambrozewicz *et al.*, Phys. Rev. C **75**, 045203 (2007).

[36] R. Nasseripour *et al.*, Phys. Rev. C **77**, 065208 (2008); D. S. Carman *et al.*, *ibid*. **79**, 065205 (2009).

[37] N. Levy, W. Majerotto, and B. J. Read, Nucl. Phys. B **55**, 493 (1973); **55**, 513 (1973); A. Bartl and W. Majerotto, *ibid*. **90**, 285 (1975).

[38] T. Mart and C. Bennhold, Nucl. Phys. A **639**, 237c (1998).

[39] O. V. Maxwell, Phys. Rev. C **76**, 014621 (2007).

[40] M. Vanderhaeghen, M. Guidal, and J.-M. Laget, Phys. Rev. C **57**, 1454 (1998); M. Guidal, J.-M. Laget, and M. Vanderhaeghen, *ibid*. **61**, 025204 (2000); **68**, 058201 (2003).

[41] B. Golli and S. Sirca, Eur. Phys. J. A **47**, 1 (2011).

[42] M. Benmerrouche, R. M. Davidson, and Nimai C. Mukhopadhyay, Phys. Rev. C **39**, 2339 (1989).

[43] W. M. Yao *et al*., J. Phys. G **33**, 1 (2006).

[44] I. J. General and S. R. Cotanch, Phys. Rev. C **69**, 035202 (2004).

[45] B. Saghai, Nucl. Phys. A **639**, 217c (1998).

[46] F. Cardarelli, I. L. Grach, I. M. Narodetskii, E. Pace, G. Salme, and S. Simula, Phys. Rev. D **53**, 6682 (1996).

[47] M. Gari and W. Krumpelmann, Z. Phys. A **322**, 689 (1985); Phys. Lett. B **173**, 10 (1986); Phys. Rev. D **45**, 1817 (1992).

[48] F. Gross and D. O. Riska, Phys. Rev. C **36**, 1928 (1987).